DOMAIN WALL MOTION IN FERROELECTRIC SWITCHING

MITSUHIKO HAYASHI

Department of Applied Physics

(Received November 13, 1972)

CONTENTS

Chapter I. Introduction

§ 1. Experimental Studies of Ferroelectric Switching

A ferroelectric can take up one of the two different polarization states (positively and negatively polarized states) and can be switched by an external electric field from one to the other of these states. It is known that the reversal of polarization is caused by the motion of the boundary or wall between the antiparallel domains.

A very frequently used method of investigating the process consists in measuring the displacement current flowing in the crystal during the reversal. The peak of the displacement current i_m or the reciprocal of the time t_s required for the switching to be completed is regarded as a measure of switching rate. A large number of measurements of the displacement current were made and it was found that the switching rates of many ferroelectrics vary with the field E following the exponential law of the form

$$i_m \propto 1/t_s \propto \exp(-\alpha/E), \tag{1.1}$$

at fields lower than a characteristic field E_1 which usually is in the neighbourhood of 2 kV/cm[1)-3)5)-12)]. The constant α in Eq. (1.1) is called the activation field. At fields higher than a field E_2 which usually is about 20 kV/cm, the switching rates of these ferroelectrics depend on E following a power law of the form

$$i_m \propto 1/t_s \propto E^n, \tag{1.2}$$

where the exponent n differs for different ferroelectrics[4)-6)8)-12)]. The field ranges $E<E_1$, $E_1<E<E_2$ and $E_2<E$ shall be called respectively the low, the intermediate and the high field range in the following. The intermediate range is the transient region from the low to the high field range.

From direct observations of the domains during switching by means of various optical techniques, it is supposed that the mechanism of polarization reversal involves the following steps[13)]; 1) nucleation of new domains, 2) forward growth of the domains through the thickness of the crystal, 3) sidewise expansion of the domains and (4) coalescence of the domains. Of these, the item (3) is most important in that most of the polarization is reversed through this process [14)-20)]. Many optical studies have been made on the sidewise motion of domain wall. Most of them concern barium titanate (BT) and it has been found[14)-19)] that the wall velocity v in this ferroelectric exhibits the same field dependence as the switching rate, *i.e.* $v=v_\infty \exp(-\delta/E)$ in the low field range and $v=kE^{1.4}$ in the high field range. Here δ is called the activation field for sidewise wall motion and approximately equal to the activation field for switching rate α. Various theoretical considerations of domain kinetics have shown[15)19)21)] that the field dependence of the switching rate follows from the field dependence of the wall velocity.

§ 2. Theoretical Studies of Ferroelectric Switching

Among the four steps of polarization reversal mentioned in the preceding section, the sidewise motion of 180° walls is the most predominant process and has been theoretically studied most in detail. It is generally agreed that a 180° wall is not very likely to move as a unit parallel to itself on an atomic scale, at least at the fields used in usual experiments. There is a certain amount of experimental evidence pointing toward an apparent sidewise wall motion caused by the nucleation and subsequent growth of reversed domains on an existing 180° wall[15)22)]. This model, which is called the nucleation model, has been theoretically studied by Miller and Weinreich[23)] and by others[24)25)].

Miller and Weinreich discussed the wall motion in BT and assumed that the

nucleus formed on an existing wall is a triangular step of dimensions l, $2a$ and c as illustrated in Fig. I.1. Here c is assumed to equal the minimum advancement of the wall. Then the dimensions and the free energy of the critical nucleus were calculated to be

$$a^* = \frac{2}{3}(\sigma''/P_sE), \tag{2.1}$$

$$l^* = 2\sigma''^{1/2}\sigma_p^{1/2}/\sqrt{3}P_sE, \tag{2.2}$$

$$\Delta F^* = \frac{8c}{3\sqrt{3}}\sigma_p^{1/2}\sigma''^{3/2}/P_sE, \tag{2.3}$$

where

$$\sigma_p = 4P_s^2 c\varepsilon_a^{-1}\ln(2a^*/eb). \tag{2.4}$$

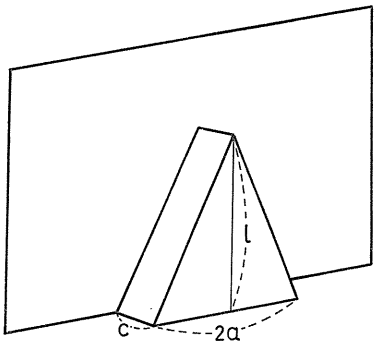

FIG. I.1. Schematic drawing of a triangular step nucleated next to a 180° domain wall.

In the equations, b is the lattice constant, P_s the spontaneous polarization, ε_a the dielectric constant in a direction perpendicular to the ferroelectric axis, σ'' the boundary energy density and e the base of the natural logarithms. As the wall velocity is proportional to the rate of nucleation on the wall, we expect that

$$v = v_\infty \exp(-\Delta F^*/kT) = v_\infty \exp(-\delta/E), \tag{2.5}$$

in agreement with the experimental result in the low field range. Here δ is given by

$$\delta = \frac{\Delta F^* E}{kT} = \frac{8c}{3\sqrt{3}}\sigma_p^{1/2}\sigma''^{3/2}/P_skT. \tag{2.6}$$

The numerical agreement between the theory and the experiment is obtained if σ'' is assumed to be 0.4 erg/cm^2 [23].

At high fields, nuclei with thicknesses greater than c may be formed. Then the wall velocity will be given by

$$v = v_\infty \sum_{n=1}^{\infty} n \exp\{-(\delta/E)n^{3/2}\}. \tag{2.7}$$

In this series, the terms with $n>1$ can be neglected in the low field range, but all terms become important in the high field range. If we sum up the series for BT, it is found that v is approximately proportional to $E^{1.45}$ at $E \approx \delta$, $E^{1.34}$ at $E \approx 100\,\delta$ and $E^{4/3}$ in the limit of $E \to \infty$. In this way, Stadler and Zachmanidis[19] successfully explained the power law in the high field range.

Experimental data are very scarce on the nucleation of new domains. There is no model theory which can account for the experimental results.

For the forward growth of spike-shaped domains, we have only one experimental data[26], according to which the velocity v_f of the forward wall motion in BT varies with E as $v_f = v_{f\infty}\exp(-\alpha_f/E)$ at fields lower than 1 kV/cm, where $v_{f\infty} = 5500$ cm/sec and $\alpha_f = 1.8$ kV/cm. The process has been discussed by Abe[27].

Assuming that the motion of the front wall is caused by successive nucleation at the steps, Abe explained the field dependence of the form $\exp(-\alpha_f/E)$.

§ 3. Discussions and the Outline of the Present Paper

The nucleation model for the sidewise wall motion is the only model which explains successfully the principal experimental results. However, all the analyses which have been made of the model, including Miller and Weinreich's, are incomplete as pointed out by Stadler[28]. Especially, the assumption that the wall velocity is proportional to the rate of nucleation on the wall of a single nucleus is open to question. If it is assumed, as Drougard did[24], that the rate controlling process is the nucleation and not the subsequent growth of the steps, the wall velocity should be proportional to the wall length. This is incompatible with the experimental fact that the wall velocity is independent of domain size. Miller and Weinreich[23] assumed, in order to overcome this difficulty, that many steps nucleate simultaneously and homogeneously along the wall and the number of nucleations per unit length of the wall is field independent. But this explanation is unsatisfactory, since perfect simultaneity and homogeneity are unreal and new nucleations may occur on the growing steps yielding a very complicated structure of steps superposing one upon another. Thus the proportionality between the wall velocity and the nucleation rate is not obvious.

Another point is that, hitherto, only the form of the field dependence of the wall velocity has been discussed by the authors and nothing has been said about the absolute value of the wall velocity. For investigating a model involving reaction rates, however, absolute discussion is of basic importance.

Thus a rigorous treatment of the problem is required, in which the step structure of the moving wall should be taken into account and the rates of all the unit reactions involved in the process should be calculated absolutely. This will be done in Chapter II, where the general formulae will be derived for the absolute wall velocity. In Chapter III, the general theory developed in Chapter II is applied to BT and various experimental results are discussed in terms of the theory. In Chapter IV, the experimentally obtained dependences on temperature and pressure of the activation fields are compared with the prediction of the theory for a number of ferroelectrics as a test for the theory.

Chapter II. Theoretical Treatment of Domain Wall Motion

§ 4. Introduction

The sidewise motion of 180° walls is the most impotant process in ferroelectric switchings. In this chapter, this process will be discussed in detail on the basis of the nucleation model, and general formulae will be derived for the absolute wall velocity. For this purpose, we first work out the kinetics of the apparent wall motion resulting from successive nucleation and growth of steps and express the wall velocity in terms of the nucleation rate and the growth velocity of the steps (§ 5). Next, we calculate the nucleation rate and the growth velocity of the steps on the basis of the theory of absolute reaction rates (§ 6 and 7). It is found that the wall velocity depends on the nucleation rate and the growth velocity of the steps in different ways for different relative magnitudes of the last two quantities. It is also shown that at very high fields two-dimensional nuclei can not nucleate and instead one-dimensional nuclei are formed,

whose nucleation rate depends on the field following a power law. Finally, combining the results thus obtained, we have the general formulae which express the absolute wall velocity in various field ranges (§ 9).

§ 5. Kinetics of Apparent Wall Motion

It will be assumed that two-dimensional nuclei nucleate on a flat 180° wall at the electrode at constant rate I per unit time and unit length of the wall and, as soon as they are formed, they begin to expand two-dimensionally on the wall with constant velocities u_s and u_f in the sideways and the forward direction, respectively. Similar nucleations may occur on the flat faces of the growing steps, thus we should have a complicated step structure. The expected complexity of a moving 180° wall is schematically illustrated in Fig. II. 1. The linear dimension in the direction of the wall motion over which the step structure extends shall be called the thickness of the moving wall.

The nucleation of the steps will increase the thickness of a moving wall, while their sideways growth tends to reduce it. Thus the thickness of a moving wall will depend on the relative effects of the two processes.

In the following, the kinetics of the wall motion resulting from the nucleation and the growth of the steps will be statistically treated for a vary thick and a very thin moving wall. Different approaches will be made for the two cases.

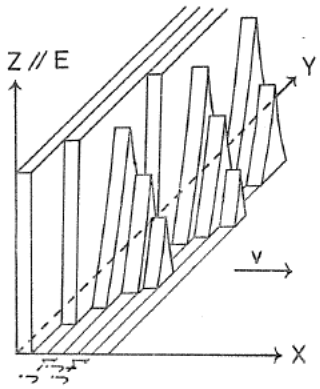

FIG. II. 1. Illustration of the step structure of a moving wall.

5.1. Thick moving wall

It is assumed that the thickness of the moving wall is large in comparison with the minimum advancement of the wall c.* The problem will be treated in two steps. First we shall discuss the two-dimensional problem in the electroded boundary surface at which the nucleations take place. Then the whole aspect of the wall motion can be visualized by combining the result of the two-dimensional problem and the growth process of the steps in the direction of the field. If the nucleation rate I and the growth velocity u_s were constant, the two-dimensional motion would be independent of the way in which the steps grow in the direction of the field. Actually, the polarization charges appearing on the boundaries of the growing steps influence the effective field at the electrode by which I and u_s are determined. Nevertheless we shall discuss in this section the two-dimensional problem on the assumption that I and u_s are fixed constants. The effect of the polarization charges will be discussed in § 8.

Let us divide the crystal into layers of thickness c and number them as illustrated in Fig. II. 1. Then we have the plane of the electrode divided into stripes. We shall define two functions of position and time which describe the two-dimensional wall motion. Let $r(j, t)$ represent the fractional length of j-th

* The minimum advancement equals the usual lattice constant when the 180° wall is perpendicular to ⟨100⟩.

stripe covered by the reversed steps at time t and $N(j,t)$ be the number of the steps per unit length of the j-th stripe at time t. Then, $r(j,t)$ should increase from zero to unity, while $N(j,t)$ increases from zero, passes through a maximum and decreases to zero again, as the wall approaches the j-th layer from a distance and leaves in the opposite direction. The functions $r(j)$ and $N(j)$ for a definite t represent in a statistical manner the instantaneous step structure of the moving wall displayed in the plane of the electrode. Since the thickness of the moving wall is assumed much greater than c, the functions $r(j)$ and $N(j)$ can be regarded as smooth functions of j although they have meaning only for integral values of j.

Now we shall seek for the differential equations which the functions $r(j,t)$ and $N(j,t)$ satisfy. For this purpose, we shall calculate the changes in r and N in j-th layer during time interval dt at time t. They can be written as

$$dr = dr_1 + dr_2, \tag{5.1}$$

$$dN = dN_1 + dN_2, \tag{5.2}$$

where the terms suffixed by 1 represent the changes caused by the sideways growth of the existing steps and those suffixed by 2 the changes due to the nucleation of new steps. It can easily be seen that dr_1 and dr_2 are expressed by

$$dr_1 = 2u_s N dt, \tag{5.3}$$

$$dr_2 = w_0 dN_2, \tag{5.4}$$

respectively, where w_0 is the width of a nucleated step at its birth. The change dN_1 is caused by the coalescence of the steps. If the interval between neighbouring steps is denoted by ξ and an exponential law* is assumed to hold for the distribution of ξ, the distribution function is expressed by $n=(N/\bar{\xi})\exp(-\xi/\bar{\xi})$, where $\bar{\xi}=(1-r)/N$ is the average interval. Hence dN_1 is evaluated as

$$dN_1 = -\int_0^{2u_s dt} n d\xi = -2u_s N^2 dt/(1-r). \tag{5.5}$$

The change dN_2 is caused by the nucleation of new steps on the $(j-1)$-th layer. The fractional length available for the nucleation is $r(j-1,t)-r(j,t)$. Thus we have

$$\begin{aligned} dN_2 &= I\{r(j-1,t) - r(j,t)\}dt \\ &= I\left\{-\frac{\partial r(j,t)}{\partial j}\right\}dt. \end{aligned} \tag{5.6}$$

From Eqs. (5.1) ~ (5.6), we obtain the following simultaneous partial differential equations which the functions $r(j,t)$ and $N(j,t)$ must satisfy:

$$\frac{\partial r}{\partial t} = 2u_s N - w_0 I \frac{\partial r}{\partial j}, \tag{5.7}$$

* This is the only distribution law having a reasonable form and leading to analytically soluble differential equations. It is shown numerically that adoption of other distribution laws such as Pearson distribution does not seriously alter the principal features of the final result.

$$\frac{\partial N}{\partial t} = -2u_s\frac{N^2}{1-r} - I\frac{\partial r}{\partial j}. \tag{5.8}$$

We are interested in a steady state of the wall motion, in which the functions $r(j)$ and $N(j)$ merely shift with a constant velocity v without changing their shapes. In such case, the functions can be written in the form:

$$r(j,t) = f(jc - vt), \tag{5.9}$$

$$N(j,t) = g(jc - vt). \tag{5.10}$$

If Eqs. (5.9) and (5.10) are inserted in Eqs. (5.7) and (5.8), we have

$$\begin{cases} f'(x) = -\dfrac{2u_s}{v - cw_0I}g(x), & (5.11) \\ g'(x) = -\dfrac{2cIu_s}{v(v-cw_0I)}g(x) + \dfrac{2u_s}{v}\dfrac{\{g(x)\}^2}{1-f(x)}, & (5.12) \end{cases}$$

where $jc - vt$ has been replaced by x. Equations (5.11) and (5.12) are the simultaneous differential equations from which the functions $f(x)$ and $g(x)$ are determined.

Fortunately, Eqs. (5.11) and (5.12) are analytically soluble (Appendix A). For the equations to have a physically reasonable solution, it is necessary that v must satisfy the condition

$$v > cw_0I. \tag{5.13}$$

For each value of v fulfilling the inequality (5.13), there exists a single definite solution which satisfies the boundary conditions:

$$f(0) = 1, \quad f(\infty) = g(0) = g(\infty) = 0. \tag{5.14}$$

If v is equal to

$$v = \eta cw_0I, \tag{5.15}$$

where η is greater than unity, the solution is expressed by

$$f(x) = 1 - \{1 - \exp(-x/\lambda)\}^{\eta}, \tag{5.16}$$

$$g(x) = \frac{1}{w_0}\exp(-x/\lambda)\{1 - \exp(-x/\lambda)\}^{\eta-1}, \tag{5.17}$$

where λ is given by

$$\lambda = \eta(\eta - 1)\frac{w_0^2I}{2u_s}c \tag{5.18}$$

and represents the thickness of the moving wall.

The right hand side of Eq. (5.16) is a monotonously decreasing function and that of Eq. (5.17) a bell-shaped function of x as expected physically. The shapes of the curves $f(x)$ and $g(x)$ are schematically illustrated in Fig. II.2. The peak value N_m of $g(x)$ is obtained by differentiating Eq. (5.17) and putting it equal to zero;

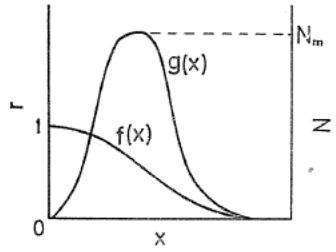

FIG. II.2. General shapes of the curves $f(x)$ and $g(x)$.

$$N_{\mathrm{m}} = (\eta - 1)^{\eta-1}/\eta^{\eta} w_0. \tag{5.19}$$

If we integrate Eq. (5.17), we obtain the total number $\mathfrak{N}$ of the steps existing per unit length of the wall;

$$\mathfrak{N} = \frac{1}{c}\int_0^{\infty} g(x)\,\mathrm{d}x = \frac{1}{2}(\eta - 1) w_0 I/u_s. \tag{5.20}$$

Existence of infinitely many steady solutions corresponding to a continuous range of a parameter ($1<\eta<\infty$) is physically unreasonable. It is shown, however, that only one of them is stable. If we solve numerically the basic equations (5.7) and (5.8)* with an arbitrary initial condition for the shapes of the functions $r(j)$ and $N(j)$ at $t=0$, we find that at sufficiently large values of t the solution reaches a steady state which is given by Eqs. (5.15) ~ (5.18) with a definite value of η which we shall call η_0.** The parameter η_0 depends on the ratio $w_0^2 I/u_s$ which is interpreted as representing the relative importance of the nucleation and the sideways growth on the wall of nuclei. The dependence is shown in Fig. II.3, which indicates that η_0 approaches unity as $w_0^2 I/u_s$ increases. However, the thickness λ is found rather small ($\lambda \approx 4c$ at $w_0^2 I/u_s = 100$ and $\lambda \approx 6c$ at $w_0^2 I/u_s = 400$), in contradiction to the assumption made at the outset that the thickness is much greater than c. This can be seen also from Eq. (5.18) in which η is now very close to unity, and suggests that the solutions are not necessarily good approximations of the real wall motion. But in spite of this discrepancy,

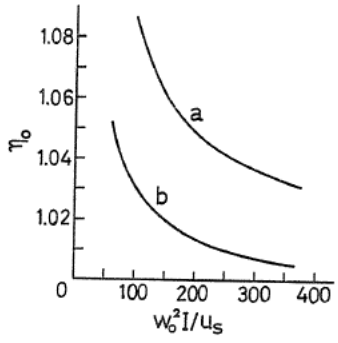

FIG. II.3. Dependence of η_0 on $w_0^2 I/u_s$. Curve *a* was determined from the study of the differential equations while curve *b* is due to the simulations.

* The equations seem to be analytically insoluble.

** If we choose for the initial condition the functions exactly expressed by Eqs. (5.16) ~ (5.18) with a value of η other than η_0, they of course remain unchanged.

the solution presents the essential features of the moving wall correctly, as is presently shown.

The problem was also studied by simulation using a computer. A wall of length 2000 times the lattice constant was considered. The nucleation on the wall was effected by adding nuclei of width w_0 and thickness c at a constant rate corresponding to I. The places of nucleation were determined by the random number method. At the same time every existing step was widened by a lattice constant at a time with a frequency which was in accordance with the relative magnitude of I and u_s. When at a place of nucleation the interval between the neighbouring steps was narrower than w_0, the possible widest nucleus was added there. Periodic condition was always maintained at both ends of the wall. The width w_0 was taken to be 10 to 100 times the lattice constant. After the wall motion reached the steady state, the velocities with which the top, the base and the 1/2-point of the wall* proceeded were evaluated and averaged.

The result shows that the steady state wall velocity v is given by the formula $v=\eta_0 c w_0 I$ with a definite value of η_0 irrespective of initial condition. The coefficient η_0 is greater than and very close to unity in the range $w_0^2 I/u_s \geq 60$ and approaches unity when $w_0^2 I/u_s$ increases (Fig. II. 3). Inspection of the step structure of the wall in the steady state reveals that the structure is fairly well represented by the functions $f(x)$ and $g(x)$ given by Eqs. (5.16) ~ (5.18) with a value of η approximately equal to 2 in the whole range of $w_0^2 I/u_s$ studied ($60< w_0^2 I/u_s <360$). The value of η determined from the comparison between Eqs. (5.18) ~ (5.20) and the results of the simulations is 2.00 ± 0.05.

Thus the results of the two methods coincide with each other as for the wall velocity in the stable steady state. However, there is a discrepancy with regard to the thickness of the moving wall. This discrepancy will be understood as follows. The differential equations require that the lower limit to the allowed value of the parameter η is unity, below which physically reasonable solutions do not exist. It is undoubted, from the results of the two methods, that for the stable steady states the η's have values very close to the lower limit. The solutions corresponding to such η's, however, can not be accepted at once as they are, since in general the properties of the solutions in a critical region are greatly affected by a slight modification in the differential equations. In the present case, the differntial equations (5.7) and (5.8) [or (5.11) and (5.12)] involve the following approximations; neglect of the discreteness of the variables, choice of a particular distribution law for the interval ξ, etc.. The simulation method also contains disputable points such as limitation due to the capacity of the computer on the sizes of the wall and the nuclei to be investigated, method of treating the nucleation at a place where the step is narrower than w_0, etc.. Nevertheless, we have ground to beleive that the result of the simulation fairly well represents the real wall motion, since the result is only slightly affected by the changes in the simulational procedure. On the other hand, the errors due to the approximations contained in the differential equations will also be small except in the critical region, hence the solutions are considered to exhibit the fundamental properties of the moving wall essentially cerrectly. From all

* The top of a wall corresponds to the value of j at which r vanishes, the base corresponds to the point at which r reaches unity and the 1/2-point is the point at which $r=1/2$.

these results it is supposed that the actual wall motion is approximated by Eqs. (5.15)~(5.20) if they are modified consulting the result of the simulation. We thus conclude that the steady state moving wall is at least approximately represented by the expressions (5.15)~(5.20), in which it is assumed that $\eta=1$ for the first and $\eta=2$ for the rest of the expressions, *i.e.*

$$v = cw_0 I, \tag{5.21}$$

$$f(x) = 1 - \{1 - \exp(-x/\lambda)\}^2, \tag{5.22}$$

$$g(x) = \frac{1}{w_0}\exp(-x/\lambda)\{1 - \exp(-x/\lambda)\}, \tag{5.23}$$

$$\lambda = \frac{w_0^2 I}{u_s}c, \tag{5.24}$$

$$N_m = 1/4w_0, \tag{5.25}$$

$$\mathfrak{N} = w_0 I/2u_s. \tag{5.26}$$

5.2. Thin moving wall

Now we shall treat a very thin moving wall, *i.e.* we assume that

$$w_0^2 I/u_s \ll 1. \tag{5.27}$$

We shall consider the wall motion in the plane of the electrode as in the preceding subsection. Let us assume that, when one layer is completely reversed, the reversed fraction of the next layer is θ_0 and N_0 steps exist per unit length of the layer on the average. Then, from the assumption (5.27), the following condition should be satisfied;

$$N_0 w_0 \ll 1. \tag{5.28}$$

If the time required for the unreversed fraction $1-\theta_0$ to be reversed is t_1, the wall velocity is written as

$$v = c/t_1, \tag{5.29}$$

where c is the minimum advancement of the wall. We shall now evaluate the time t_1. Under the present condition the unreversed fraction $1-\theta_0$ will be large enough so that many further nucleations occur before the layer is completely reversed. The kinetics of nucleation and growth of steps in a single layer can be treated by Avrami's theory[29)-31)] applied to one-dimensional problem. According to the theory, the extended reversed fraction A of a layer which is calculated neglecting the overlapping of the growing steps is related with the true reversed fraction θ by the approximate formula

$$d\theta/dA = 1 - \theta. \tag{5.30}$$

The integration of Eq. (5.30)

$$\int_{\theta_0}^{\theta}\frac{d\theta}{1-\theta} = \int_{A_0}^{A} dA$$

yields

$$\theta = 1 - (1 - \theta_0) \exp(A_0) \exp(-A), \tag{5.31}$$

where A_0 is the extended reversed fraction corresponding to θ_0.* The extended fraction A at time t after the completion of the reversal of the preceding layer is written as

$$\begin{aligned} A(t) &= A_0 + 2N_0 u_s t + w_0 I t + \int_0^t 2u_s I(t-\tau)\mathrm{d}\tau \\ &= A_0 + 2N_0 u_s t + w_0 I t + u_s I t^2. \end{aligned} \tag{5.32}$$

According to Eqs. (5.31) and (5.32), an infinite time is necessary for θ to reach unity. Actually, however, a layer is reversed within a finite time. This discrepancy is due to the fact that Eq. (5.30) is only an approximate expression. Therefore we shall assume that the reversal is completed when

$$\theta = 1 - (1 - \theta_0)\varepsilon, \tag{5.33}$$

where ε is a positive number which is small in comparison with unity. Then $\theta(t_1) = 1 - (1-\theta_0)\varepsilon$ and we have

$$A(t_1) = \rho - \theta_0 + A_0 \tag{5.34}$$

from Eq. (5.31), where

$$\rho = -\ln\{(1 - \theta_0)\varepsilon\}. \tag{5.35}$$

Substituting t_1 for t in the right hand side of Eq. (5.32), putting it equal to $\rho - \theta_0 + A_0$ in accordance with Eq. (5.34) and solving for t_1, we have

$$w_0 I t_1 = \frac{-\left(1 + \frac{2N_0 u_s}{w_0 I}\right) + \sqrt{\left(1 + \frac{2N_0 u_s}{w_0 I}\right)^2 + 4\frac{u_s}{w_0^2 I}(\rho - \theta_0)}}{2\frac{u_s}{w_0^2 I}}. \tag{5.36}$$

Under the condition (5.28), it is found that

$$N_0 u_s / w_0 I \ll u_s / w_0^2 I, \tag{5.37}$$

$$(N_0 u_s / w_0 I)^2 \ll u_s / w_0^2 I. \tag{5.38}$$

Thus, when the condition (5.27) is satisfied, only the second term in the square root should be retained in the numerator on the right hand side of Eq. (5.36), and the equation is approximated by

$$w_0 I t_1 = (\rho - \theta_0)^{1/2} w_0 (I/u_s)^{1/2}. \tag{5.39}$$

Thus, from Eqs. (5.29) and (5.39), we obtain

$$v = (\rho - \theta_0)^{-1/2} c (u_s I)^{1/2}. \tag{5.40}$$

* The determination of the appropriate value of A_0 is a rather complicated problem, but fortunately its value has no influence on the final result as can be seen from Eqs. (5.31) or (5.36).

Study by simulation reveals that the wall velocity v is represented very well by the formula

$$v = 1.4\, c(u_s I)^{1/2} \tag{5.41}$$

for the values of $w_0^2 I/u_s$ ranging from 10^{-4} to 1/20. The numerical coefficient on the right hand side of Eq. (5.41) obtained from the whole data of the simulation is 1.44 ± 0.04. Comparison of Eqs. (5.40) and (5.41) indicates that $\rho - \theta_0 = 0.51$, which corresponds to $\varepsilon = 0.6$ in accordance with Eq. (5.35). The simulation also reveals that the step structure extends over a few layers at $w_0^2 I/u_s \approx 10^{-4}$ and the wall thickness increases with increasing $w_0^2 I/u_s$, reaching about ten layers at $w_0^2 I/u_s \approx 10^{-2}$. The average reversed fraction θ_0 is found to be of the order of 0.2 at $w_0^2 I/u_s \approx 10^{-4}$, increases with increasing $w_0^2 I/u_s$ and reaches about 0.7 at $w_0^2 I/u_s \approx 10^{-2}$.

§ 6. Rate of Nucleation on a wall

As described in § 1, the field dependence of the switching rate follows an exponential law in the low field range and a power law in the high field range. The different field dependences of the switching rate in the different field ranges are explained by the present theory in terms of the difference in the mechanism of the nucleation on an existing wall. In this section the nucleation rate on a wall is calculated in the low and the high field range.

We shall follow the way in which Turnbull and Fisher[32] derived an expression for the absolute rate of nucleation in condensed systems. Nuclei are assumed to grow one unit cell at a time. Only the nuclei which have exceeded the critical size can grow freely. The steady state rate of nucleation corresponds to constant equal net forward rate for the set of reactions:

$$m\alpha_1 \rightleftarrows \beta_m, \quad \beta_m + \alpha_1 \rightleftarrows \beta_{m+1}, \quad \beta_{m+1} + \alpha_1 \rightleftarrows \beta_{m+2}, \quad \ldots \tag{6.1}$$

where α_1 represents an unreversed unit cell, β_i a reversed nucleus containing i unit cells and β_m the smallest nucleus.

6.1. Nucleation rate in the low field range

We shall assume that the shape of a growing two-dimensional nucleus is constant. This assumption is adequate as can be seen from the energy contours as shown in Fig. II. 4. Then, the increment in free energy associated with the formation of a nucleus containing i unit cells (β_i) is expressed in the form

$$\Delta F_i/kT = A_0 + Ai^{1/2} - Bi. \tag{6.2}$$

In the right hand side of Eq. (6.2), the first and the second term represent the combined effect of the boundary and the depolarization energy and the third term is due to the bulk energy (Appendix C). The size and the free energy of the critical nucleus are respectively

$$i^* = (A/2B)^2 \tag{6.3}$$

and

$$\Delta F^*/kT = A_0 + A^2/4B. \tag{6.4}$$

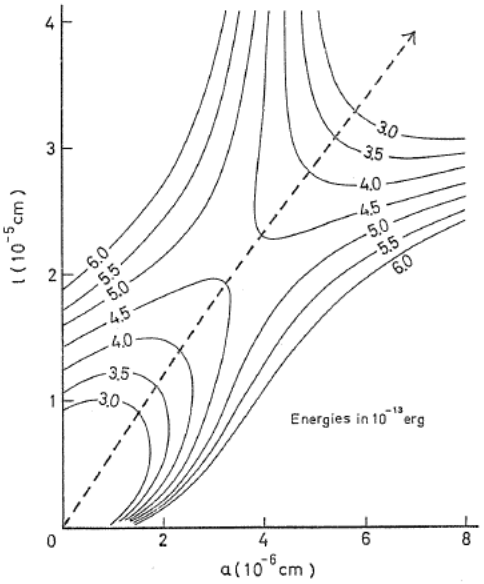

FIG. II.4. Free energy contours for a triangular nucleus of height l and base $2a$. This is the plot of the right hand side of Eq. (C.1) omitting U_Γ. Employed constants are $b=4$ A, $P_s=7.8\times10^4$ esu, $\sigma''=0.4$ erg/cm^2, $\varepsilon_a=\varepsilon_b\sim2000$, $\varepsilon_c=120$ and $E=1$ esu. (These are the accepted values for BT.)

Let us consider the reaction $\beta_i+\alpha_1\rightleftarrows\beta_{i+1}$. If n_i represents the steady state linear concentration of β_i nuclei along the wall, the rates of the forward and the reverse reaction are written as

$$r^+=n_i s_1 i^{1/2}(kT/h)\exp(-\Delta f_1^*/kT) \tag{6.5}$$

and

$$r^-=n_{i+1}s_2 i^{1/2}(kT/h)\exp(-\Delta f_2^*/kT), \tag{6.6}$$

respectively, according to the theory of absolute reaction rates[33]. Here $s_1 i^{1/2}$ and $s_2 i^{1/2}$ are the numbers respectively of the unreversed and the reversed unit cells existing along the boundary of a nucleus and hence available for the reactions, Δf_1^* and Δf_2^* the energy barriers corresponding to the activated complex (Fig. II.5) and h is the Planck constant. The net forward rate of the reaction is

$$r^*=r^+-r^-=-(skT/h)\exp(-\Delta f^*/kT)i^{1/2}\left[n_i\frac{\mathrm{d}(\Delta F_i)}{\mathrm{d}i}/kT+\frac{\mathrm{d}n_i}{\mathrm{d}i}\right]. \tag{6.7}$$

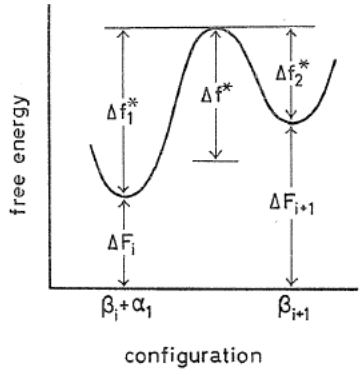

FIG. II.5. Free energy barrier between $\beta_i+\alpha_1$ and β_{i+1}.

Here we have assumed that $s_1 \approx s_2 = s$, n_i and ΔF_i are smooth functions of i and $\{d(\Delta F_i)/di\}/kT$ and $(dn_i/di)/n_i$ are small in comparison with unity. The free energy difference between the activated complex and the mean of ΔF_i and ΔF_{i+1} is denoted by Δf^* (Fig. II.5).

If we put

$$R = r^*/(skT/h)\exp(-\Delta f^*/kT), \tag{6.8}$$

then Eq. (6.7) reduces to the differential equation

$$\frac{dn_i}{di} + \left[\frac{d(\Delta F_i)}{di}/kT\right] n_i + Ri^{-1/2} = 0. \tag{6.9}$$

The solution is

$$n_i = \exp\left(-\frac{\Delta F_i}{kT}\right)\left[-R\int_{i_0}^{i} i^{-1/2}\exp\left(\frac{\Delta F_i}{kT}\right)di + n_1\right], \tag{6.10}$$

where n_1 is the linear concentration of unit cells along the wall. The constant of integration has been determined from the boundary condition that n_i coincides for sufficiently small i's with the equilibrium concentration assuming no nucleation.

Since $\Delta F_i \to -\infty$ when $i \to \infty$ and it is required that $n_i \to 0$ when $i \to \infty$, it must follow that

$$R = n_1 / \int_{i_0}^{\infty} i^{-1/2}\exp\left(\frac{\Delta F_i}{kT}\right)di. \tag{6.11}$$

The exact location of the lower limit of the integration in Eq. (6.11) is unimportant. Using Eq. (6.2) and neglecting the higher order terms in Taylor's expansion, the integral is evaluated as

$$\int_0^{\infty} i^{-1/2}\exp\left(\frac{\Delta F_i}{kT}\right)di = \left(\frac{8\pi}{A}\right)^{1/2} i^{*1/4}\exp\left(\frac{\Delta F^*}{kT}\right). \tag{6.12}$$

Thus we have, from Eqs. (6.8), (6.11) and (6.12),

$$I = r^* = n_1(kT/h)(A/8\pi)^{1/2} s i^{*-1/4}\exp\{-(\Delta f^* + \Delta F^*)/kT\} \tag{6.13}$$

for the steady state rate of nucleation.

The quantities A, s, i^* and $\Delta F^*/kT$ for a triangular nucleus are given by (Appendix C)

$$A = (8/3^{3/4}) b_x (b_y b_z)^{1/2} \sigma''^{3/4} \sigma_p^{1/4}/kT, \tag{6.14}$$

$$s = 2(3\sigma_p/\sigma'')^{1/4}, \tag{6.15}$$

$$i^* = (4/3^{3/2})\sigma''^{3/2}\sigma_p^{1/2}/b_y b_z P_s^2 E^2, \tag{6.16}$$

$$\Delta F^*/kT = U_f/kT + \delta/E. \tag{6.17}$$

Here b_x, b_y and b_z are the three lattice constants when the crystal axes are taken parallel to x, y and z-direction of Fig. II.1,* P_s is the spontaneous polarization,

* The lattice constant b_x equals the minimum advancement of the wall c.

σ'' the energy density of the side boundary of the steps, U_f the extra energy existing at the top of a step and σ_p and δ are given by (Appendices B and C)

$$\sigma_p = \frac{4P_s^2 b_x}{(\varepsilon_a\varepsilon_b)^{1/2}}\left[\ln\left\{\left(\frac{2}{\mu}\right)^{1/2}\frac{(\varepsilon_a\varepsilon_b)^{3/4}}{\varepsilon_c(\varepsilon_a\cos^2\varphi+\varepsilon_b\sin^2\varphi)^{1/2}}\frac{l^{*2}}{a^*(b_xb_y)^{1/2}}\right\}-2\ln 2\right], \tag{6.18}$$

$$\delta = (8/3^{3/2})b_x\sigma''^{3/2}\sigma_p^{1/2}/P_skT, \tag{6.19}$$

where ε_a, ε_b and ε_c are the dielectric constants in the directions of the principal axes (a, b and c) of the dielectric ellipsoid of the crystal, φ is the angle between the a- and the x- axis in the xy- (or ab-) plane,* l^* and $2a^*$ are the height and the width, respectively, of the critical nucleus and μ represents the thickness of the slanting side boundaries measured in b_y.

Thus Eq. (6.13) can be rewritten in the form

$$I = I_0E^{1/2}\exp(-\delta/E), \tag{6.20}$$

where

$$I_0 = \left(\frac{2\sqrt{3}}{\pi}\right)^{1/2}\frac{(kT)^{1/2}}{h}(b_xb_yb_z)^{1/2}P_s^{1/2}\left(\frac{\sigma_p}{\sigma''}\right)^{1/4}n_1\exp\left(-\frac{\Delta f^*}{kT}\right)\exp\left(-\frac{U_f}{kT}\right). \tag{6.21}$$

6.2. Nucleation rate in the high field range

The critical size of the two-dimensional nuclei decreases with the increasing field. If the size of a nucleus is treated macroscopically except for the thickness, the critical width a^* is found to be of the order of σ''/P_sE for any shape of the nucleus provided its width is small in comparison with the height. Here σ'' represents the average energy density of the side boundary of the nucleus. At fields higher than

$$E'' = \sigma''/P_sb, \tag{6.22}$$

the width a^* is smaller than the lattice constant b, thus the semi-macroscopic treatment fails and the two-dimensional nuclei can not nucleate. On the other hand, if the energy density of the front boundary of a nucleus is generally denoted by σ_f, the critical height of the fictitious nucleus is of the order of σ_f/P_sE. This is much greater than b in a considerable range of field above E'' since σ_f is much greater than σ''. We shall therefore assume that, in this field range, one-dimensional nuclei nucleate, which will grow two-dimensionally on the wall after the nucleation.

The critical field E'' given by Eq. (6.22) must be closely related with the characteristic fields E_1 and E_2 separating the three field ranges defined in §1 from each other. The relation will be roughly expressed by the inequality

$$E_1 \ll E'' \lesssim E_2. \tag{6.23}$$

Now we shall calculate the nucleation rate of the one-dimensional nuclei. The increase in free energy associated with the formation of a one-dimensional

* In many ferroelectrics including BT, TGS, etc., the ferroelectric axis coincides with one of the principal crystallographic axes. Except for triclinic crystals, the latter in turn coincides with one of the principal axes of the dielectric ellipsoid which we call the c-axis. Equations (6.18) and (6.19) are applicable to such cases.

nucleus of length $ib_z(\beta_i)$ is

$$\Delta F_i = b_x b_y(\sigma_f + \sigma_p') - 2b_x b_z(EP\, b_y - \sigma')i, \tag{6.24}$$

where σ' and σ_f are the energy densities of the side and the front boundary, respectively,* and σ_p' is given by (Appendix B)

$$\sigma_p' = \frac{P_s^2 b_x b_y}{2\pi(\varepsilon_a\varepsilon_b)^{1/2}\nu b_z}\ln\frac{4(\varepsilon_a\varepsilon_b)^{1/4}\nu b_z}{\varepsilon_c^{1/2}(b_x b_y)^{1/2}}. \tag{6.25}$$

Here ν represents half the thickness of the front boundary measured in b_z. The other symbols bear the same meanings as in the preceding subsection.

We shall rewrite Eq. (6.24) as

$$\Delta F_i/kT = C - Di, \tag{6.26}$$

with

$$C = b_x b_y(\sigma_f + \sigma_p')/kT, \tag{6.27}$$

$$D = 2b_x b_z(EP_s b_y - \sigma')/kT. \tag{6.28}$$

For fields of interest, for which the semi-macroscopic treatment of nuclei fails, the coefficient D is positive. At much lower fields, two-dimensional nuclei nucleate and discussion has already been made in the preceding subsection. The intermediate range of field is the transient region.

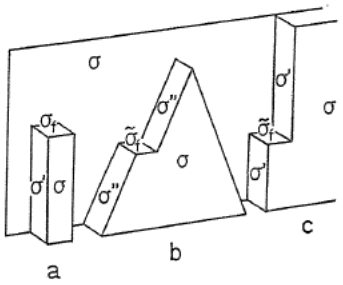

FIG. II.6. Symbols representing the energy densities of various kinds of boundaries.

Equation (6.26) represents a linear function of i if the constants C and D are really constant. Actually, however, for small i's, the spontaneous polarization and hence the boundary energies σ' and σ_f are smaller than the bulk values and vanish at the limit of $i=0$, thus the curve $\Delta F_i/kT$ versus i deviates from the straight line representing the relation at large i's (Fig. II.7). The critical size $i\dagger$ will be of the same order as the thickness of the front boundary.

The forward, the reverse and the net reaction rate for the reaction $\beta_i + \alpha_1 \rightleftharpoons \beta_{i+1}$ are given, this time, by

* In the present paper, the 180° wall energy is represented by σ, the vertical side boundary energy of a step nucleus by σ', the slanting side boundary energy by σ'' and the front boundary energy of a one-dimensional step by σ_f or $\tilde{\sigma}_f$ according as it is isolated or adjacent to an existing step (Fig. II.6).

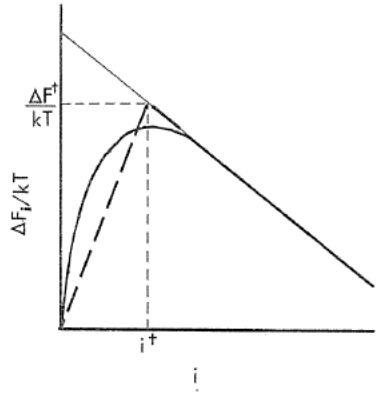

FIG. II.7. Free energy ΔF_i of one-dimensional nucleus as a function of its size i. The curved portion is approximated by the broken straight line for the calculation.

$$r^+ = n_i(kT/h)\exp(-\Delta f_1^\dagger/kT), \tag{6.29}$$

$$r^- = n_{i+1}(kT/h)\exp(-\Delta f_2^\dagger/kT) \tag{6.30}$$

and

$$r^* = r^+ - r^- = -(kT/h)\exp(-\Delta f^\dagger/kT)\left[n_i\frac{\mathrm{d}(\Delta F_i)}{\mathrm{d}i}/kT + \frac{\mathrm{d}n_i}{\mathrm{d}i}\right], \tag{6.31}$$

respectively, with the same notations as in the preceding subsection except for the energy barriers which are now denoted by $\Delta f^\dagger$, $\Delta f_1^\dagger$ and $\Delta f_2^\dagger$.

If we put

$$R = r^*/(kT/h)\exp(-\Delta f^\dagger/kT), \tag{6.32}$$

and proceed in the same way as before, solving a differential equation for n_i and considering the requirement that $n_i \to 0$ when $i \to \infty$, we find

$$R = n_1/\int_0^\infty \exp(\Delta F_i/kT)\mathrm{d}i. \tag{6.33}$$

Since the exact shape of the curved portion of Fig. II.7 is unknown, we shall represent the curve $\Delta F_i/kT$ versus i by the following approximate expression:

$$\Delta F_i/kT = \begin{cases} C - Di, & (i > i^\dagger) \\ Gi, & (i < i^\dagger) \end{cases} \tag{6.34}$$

where

$$G = (C - Di^\dagger)/i^\dagger. \tag{6.35}$$

In Eqs. (6.34) and (6.35), C and D are the constants defined by Eqs. (6.27) and (6.28) with the bulk values of σ', σ_t and P_s. The approximation expressed by Eq. (6.34) is shown by the broken line in Fig. II.7.

The integral in Eq. (6.33) can then be evaluated as

$$\int_0^\infty \exp(\Delta F_i/kT)\mathrm{d}i = \frac{kT}{\Delta F^\dagger}\left[\frac{C}{D}\exp(\Delta F^\dagger/kT) - i^\dagger\right]. \tag{6.36}$$

Here

$$\Delta F^{\dagger} = kT(C - Di^{\dagger}) \tag{6.37}$$

represents the approximate critical free energy (Fig. II.7).

We thus obtain, from Eqs. (6.32), (6.33) and (6.36),

$$I = r^{*} = \frac{n_1}{h}\exp(-\Delta f^{\dagger}/kT)\Delta F^{\dagger}\left[\frac{C}{D}\exp(\Delta F^{\dagger}/kT) - i^{\dagger}\right]^{-1} \tag{6.38}$$

for the steady state rate of nucleation. Using Eqs. (6.27), (6.28) and (6.37), we can rewrite Eq. (6.38) in the form

$$I = \frac{n_1 b_x b_y}{h}\exp(-\Delta f^{\dagger}/kT)\{\sigma_f + \sigma_p' - 2i^{\dagger}P_s b_z(E - E')\}$$
$$\times\left[\frac{\sigma_f + \sigma_p'}{2P_s b_z(E-E')}\exp\{b_x b_y(\sigma_f + \sigma_p')/kT\}\exp\{-2i^{\dagger}P_s b_x b_y b_z(E - E')/kT\} - i^{\dagger}\right]^{-1}, \tag{6.39}$$

where

$$E' = \sigma'/P_s b_y. \tag{6.40}$$

Numerical investigation of Eq. (6.39) using reasonable values of the constants reveals that the relation between I and E is very closely expressed by a power law of the form

$$I = I_0' E^{n} \tag{6.41}$$

in the range of E of interest. The exponent n depends on the critical size $i^{\dagger}$ and the boundary energies σ' and σ_f. An example of the numerical calculation is shown in Fig. II.8, in which $i^{\dagger}$, σ' and σ_f are assumed to be 6.4, 0.205 erg/cm^2 and 41.1 erg/cm^2, respectively, then n is found to be 1.54.*

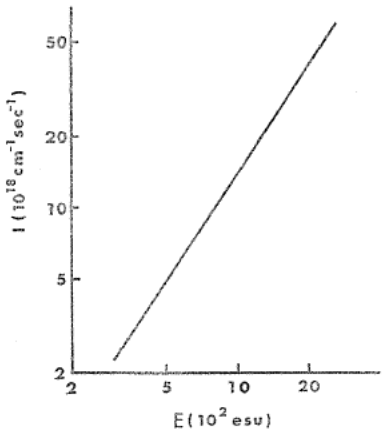

FIG. II.8. Nucleation rate I versus field E in the high field range. This is the plot of Eq. (6.39). Constants for BT were employed, in particular $i^{\dagger}$, σ' and σ_f were taken to be 6.4, 0.205 erg/cm^2 and 41.1 erg/cm^2, respectively.

It should be noted that the above treatment is valid only within a finite range of field avove E'', since at fields exceeding the order of $\sigma_f/P_s b$ the critical

* These values are appropriate to BT (next chapter). The other constants are also fitted to BT in the calculation.

free energy $\Delta F\dagger$ is negative as can be seen from Eqs. (6.27), (6.28) and (6.37). We have, however, no experimental data at such high fields.

§7. Velocity of Two-Dimensional Growth of Nucleus on a Wall

Before a nucleated step much exceeds the critical size, the mechanism of its two-dimensional growth will be similar to that of the pre-nucleation process; a growing nucleus will be nearly in thermal equilibrium with the surroundings at every instant of time and the growth will proceed along the valley of the free energy surface as indicated by the dotted line in Fig. II.4.

After the step has grown much larger than the critical size, its further growth can not be the quasi-equilibrium process and the motion of every part of it is now determined by the local condition.

It is expected that a nucleated step quickly leaves the quasi-equilibrium state and most of its two-dimensional growth is through the process of the latter type. Therefore, we consider only such process in the following.

7.1. *Sideways growth velocity*

It is very unlikely at fields of interest that a side boundary moves as a unit which is parallel to itself. This is for the same reason as a 180° wall can not move as a unit. So we shall examine another model, *i.e.*, apparent motion of the side boundary due to nucleation adjacent to it.

If we study the energy contours for the two-dimensional nuclei of various shapes with width ξ and height η nucleating adjacent to an existing step, it is found that the critical point is always located on the η-axis. Thus we shall assume that a one-dimensional nucleus is first formed (Fig. II.9).

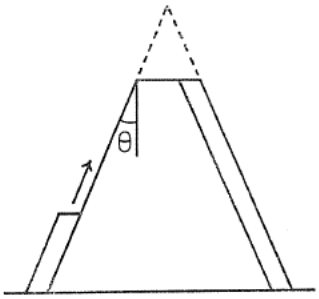

FIG. II.9. Illustration of one-dimensional nuclei formed adjacent to an existing step and the forward growth of the step as the result of the successive nucleation and growth of the nuclei.

Then, the problem is very similar to that treated in §6.2, and we can argue along the same line as before, obtaining

$$r^* = \frac{2b_x b_y}{h}\exp(-\Delta\tilde{f}^\dagger/kT)\cdot\{\tilde{\sigma}_f+\sigma_p'-2\tilde{i}^\dagger P_s b_z E\}\left[\frac{\tilde{\sigma}_f+\sigma_p'}{2P_s b_z E}\right.$$
$$\left.\times\exp\{b_x b_y(\tilde{\sigma}_f+\sigma_p')/kT\}\exp(-2\tilde{i}^\dagger P_s b_x b_y b_z E/kT)-\tilde{i}^\dagger\right]^{-1} \qquad (7.1)$$

for the rate at which a one-dimensional nucleus is formed on one of the side boundaries of an existing step. Here $\tilde{i}^\dagger$, $\tilde{\sigma}_f$ and $\Delta\tilde{f}^\dagger$ represent the critical size corresponding to the maximum free energy, the energy density of the front boundary and the energy barrier for unit advancement of the front boundary,

respectively, of the one-dimensional nucleus adjacent to an existing step, and σ_p' is given by Eq. (6.25). The validity of Eq. (7.1) is restricted to the field range $E \lesssim \tilde{\sigma}_f / P_s b$ for the same reason as mentioned at the end of § 6.2.

A nucleated one-dimensional nucleus may continue the one-dimensional growth or it may grow, after it exceeded the critical height of the fictitious two-dimensional nucleus, along the valley of the free energy surface increasing its width. A simple calculation indicates that the latter process is unimportant as compared with the former.* Hence it is expected that the sideways growth of an existing step is mostly brought about by the successive nucleation and forward growth of the one-dimensional nuclei adjacent to it. Thus, from Eq. (7.1), the velocity of the sideways growth of a step is written as

$$u_s = b_y r^* = \frac{2 b_x b_y^2}{h} \exp\left(-\Delta \tilde{f}^\dagger / kT\right) \cdot \{\tilde{\sigma}_f + \sigma_p' - 2 \tilde{i}^\dagger P_s b_z E\}$$
$$\times \left[\frac{\tilde{\sigma}_f + \sigma_p'}{2 P_s b_z E} \exp\{b_x b_y (\tilde{\sigma}_f + \sigma_p')/kT\} \exp\left(-2 \tilde{i}^\dagger P_s b_x b_y b_z E / kT\right) - \tilde{i}^\dagger\right]^{-1}. \quad (7.2)$$

In the low field range, the second term in the square bracket can be neglected against the first and it can be written that $2 \tilde{i}^\dagger P_s b_x b_y b_z E / kT \ll 1$ and $2 \tilde{i}^\dagger P_s b_z E \ll \tilde{\sigma}_f + \sigma_p'$, since $E \ll \sigma'' / P_s b$ in this field range as is indicated by Eq. (6.22) and inequality (6.23) and σ'' is much smaller than $\tilde{\sigma}_f$. Thus Eq. (7.2) is simplified:

$$u_s = \frac{4 P_s b_x b_y^2 b_z}{h} \exp\left(-\Delta \tilde{f}^\dagger / kT\right) \exp\{-b_x b_y (\tilde{\sigma}_f + \sigma_p')/kT\} \cdot E. \quad (7.3)$$

Numerical calculation using reasonable values of the constants shows that the right hand sides of Eqs. (7.2) and (7.3) vary with E approximately following a power law.

7.2. Forward growth velocity

According to Eqs. (5.21) and (5.41), the wall velocity v does not depend on the forward growth velocity u_f of the steps, although actually the latter has an influence on the former through the polarization charge effect, which, however, is usually unimportant (§ 8). Nevertheless we shall briefly discuss the forward growth of the steps.

Let us first calculate the velocity of the forward growth of the one-dimensional side nucleus about which we have just discussed. The front boundary of the nucleus is considered to proceed taking the even and the odd state** alternately. Thus the potential barrier which the boundary must surmount to advance a unit distance is equal to the difference between the energies corresponding to the two states, which we shall denote as ΔU (Fig. II.10). The decrease in free energy associated with the unit advancement of the boundary equals $\Delta F' = 2 E P_s b_x b_y b_z$ (Fig. II.10). Thus the velocity of the forward growth of the one-dimensional

* The sideways growth velocity of the nucleus due to the second process is calculated to be of the order of $(2 P_s b^5 / hl) \exp(-\Delta \tilde{f}^\dagger / kT) E$, which is smaller than the velocities given by Eqs. (7.3) and (7.4) by a factor of approximately b/l, where l is the height of the growing nucleus. The exponential factors appearing in these expressions are of the order of unity.

** A front boundary is referred to as being in even or odd state, according as it consists of even or odd number of lattices.

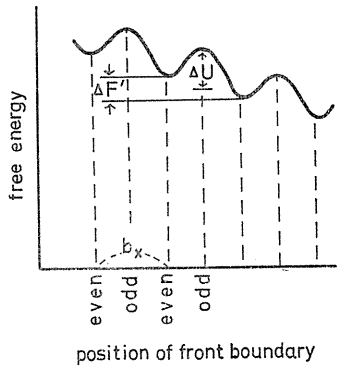

FIG. II.10. Potential barrier for the forward growth of a one-dimensional nucleus.

side nucleus is given by

$$u' = b_z(r^+ - r^-) = \frac{b_z}{h}\Delta F' \exp(-\Delta U/kT) = \frac{2P_s b_x b_y b_z^2}{h}\exp(-\Delta U/kT)\cdot E, \qquad (7.4)$$

where

$$r^+ = (kT/h)\exp\left\{-\left(\Delta U - \frac{1}{2}\Delta F'\right)/kT\right\}, \qquad (7.5)$$

$$r^- = (kT/h)\exp\left\{-\left(\Delta U + \frac{1}{2}\Delta F'\right)/kT\right\}. \qquad (7.6)$$

Thus one-dimensional nuclei formed adjacent to an existing step rapidly grow forward and widen the top of the step creating a flat front boundary as shown in Fig. II.9. Then the probability must be very high that a triangular top as shown by the dotted line in the figure is added to the step, since by that process the flat front boundary with very high energy density is replaced by the slanting boundaries having much lower energy density and free energy is gained by the addition of the reversed volume. In this way the top of an existing step proceeds as the result of successive nucleation and forward growth of the one-dimensional side nuclei.

It will be assumed that the side boundaries of a growing step have a definite slanting angle θ, which corresponds to the energetically optimum condition and is maintained throughout the growth.* Then the ratio of the forward to the sideways growth velocity of a step is eqaul to cot θ (Fig. II.9). Thus we have, for the forward growth velocity,

$$u_f = u_s \cot\theta = \frac{2b_x b_y^2}{h}\cot\theta \exp(-\Delta\tilde{f}^\dagger/kT)\cdot\{\tilde{\sigma}_f + \sigma_p' - 2\tilde{i}^\dagger P_s b_z E\}$$
$$\times\left[\frac{\tilde{\sigma}_f + \sigma_p'}{2P_s b_z E}\exp\{b_x b_y(\tilde{\sigma}_f + \sigma_p')/kT\}\exp(-2\tilde{i}^\dagger P_s b_x b_y b_z E/kT) - \tilde{i}^\dagger\right]^{-1}. \qquad (7.7)$$

* After the step has grown through the thickness of the crystal, the angle θ will almost vanish. Thus, strictly, $\tilde{\sigma}_f$ and hence u_s differ for the steps having grown through the thickness (c of Fig. II.6) and for the ones during growth (b of Fig. II.6). In Eq. (7.7), the u_s and the $\tilde{\sigma}_f$ for the latter should be employed, while those in Eqs. (7.2) and (7.3) should be taken as suitable averages taken between the two types of steps.

§8. Effect of Polarization Charges

Principal part of the polarization charges will be those existing on the slanting side boundaries of the growing steps. We shall consider only such charges and estimate their effect on the wall motion in a simplified manner.

When $w_0^2 I/u_s \ll 1$, the moving wall is very thin, thus the thickness of the wall can be neglected in calculating the field E_p which is created near the electrode by the polarization charges and is opposite in direction to the applied field E. The field E_p can be regarded as being caused by a surface charge distributed on the wall, the density q_s of which is a function of the height z measured from the electrode and decreases rapidly with z. We shall assume that function $q_s(z)$ can be written as

$$q_s = C/z^\gamma, \tag{8.1}$$

where γ is assumed to be positive and independent of the field. It will be difficult to determine the exact value of γ since the problem is so complicated. Fortunately, its value does not affect seriously the result. The constant C can be determined from the condition that $q_s = \rho N_B$ at $z = l^*$, where ρ is the linear density of the polarization charge along a side boundary of a step, N_B the total number of the boundaries per unit length of the wall and l^* the height of the critical nucleus. We obtain

$$C = \rho N_B l^{*\gamma}. \tag{8.2}$$

Since $q_s(z)$ is a rapidly decreasing function of z, the field E_p is mostly due to the charges near the electrode. Therefore, the length of the wall is unimportant and we can write

$$\begin{aligned} E_p &= \frac{2}{\varepsilon}\int_{l^*}^{d} \frac{q_s \mathrm{d}z}{z} \\ &= \frac{2C}{\varepsilon\gamma}\left(\frac{1}{l^{*\gamma}} - \frac{1}{d^\gamma}\right) \approx \frac{2C}{\varepsilon\gamma l^{*\gamma}}, \end{aligned} \tag{8.3}$$

where d is the thickness of the crystal. The lower limit of integration has been taken to be l^*, since the charges between $z=0$ and $z=l^*$ have no effect, on the average, on the nucleation of a nucleus of height l^*.

The linear density ρ is written as

$$\rho = 2 P_s b_x \tan\theta, \tag{8.4}$$

where θ is the slanting angle of the side boundaries. It can be shown that (Appendix D)

$$N_B \lesssim 2(I/u_s)^{1/2}. \tag{8.5}$$

Thus the upper limit to E_p is determined, from Eqs. (8.2) ~ (8.5):

$$E_p \lesssim 8 P_s b_x (I/u_s)^{1/2} \tan\theta/\varepsilon\gamma. \tag{8.6}$$

When $w_0^2 I/u_s \gg 1$, we have a thick moving wall and E_p is caused by a volume charge distributed in the moving wall of finite thickness ($\approx\lambda$). We shall assume

that the volume density q_v is a function of the height z only and can be expressed as

$$q_v = C'/z^\gamma, \tag{8.7}$$

with the same γ as in Eq. (8.1). The charge density q_v should equal $\rho N_B/\lambda$ at $z=l^*$, hence the constant C' is determined to be

$$C' = \rho N_B l^{*\gamma}/\lambda. \tag{8.8}$$

This time the number N_B is equal to $2\mathfrak{N}$, where $\mathfrak{N}$ is given by Eq. (5.26).

The field E_p at the mid point through the thickness of the wall is given by

$$E_p = \frac{C'}{\varepsilon}\int_{-\lambda/2}^{\lambda/2}\int_{-\infty}^{\infty}\int_{l^*}^{d}\frac{dxdydz}{z^\gamma(x^2+y^2+z^2)}\cos\alpha. \tag{8.9}$$

The meaning of the symbols are indicated in Fig. II. 11.

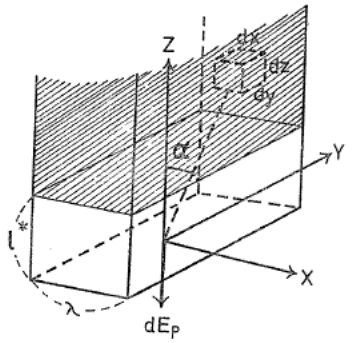

FIG. II. 11. Opposite field E_p produced by a volume charge distributed in a moving wall of thickness λ.

Numerical calculations show that usually the right hand side of inequality (8.6) is quite negligible against the applied field E. For a thick moving wall, the field E_p given by Eq. (8.9) is not always negligible as compared to E. However, its influence is not serious in most cases.*

It should be pointed out that the effect of polarization charge is overestimated in this section, since we have not taken into account the compensation of the polarization charges by the free charges within the crystal.

§9. Absolute Wall Velocity

In this section we shall obtain the expressions for the absolute wall velocity, combining the results of §5~7. The nucleation rate I depends exponentially on the field E in the low field range (§6), while the growth velocity u_s varies much more slowly with E (§7). Hence it is expected that at sufficiently low fields the effect of I is small as compared with that ot u_s, *i.e.* $w_0^2 I/u_s \ll 1$. With increasing field, the nucleation rate I increases very rapidly and its effect will come to predominate over that of u_s, making $w_0^2 I/u_s$ much greater than unity. At very high fields, however, the relative effectiveness of I and u_s may be reversed and we shall have $w_0^2 I/u_s \ll 1$ again since the rapidity with which I varies with E

* Numerical discussion of these effects will be made for BT in the next chapter.

diminishes (§6) and the critical width w_0 of a nucleus decreases with E [Eq. (2.1)]. Thus we shall assume that $w_0^2 I/u_s \ll 1$ at very low fields, $w_0^2 I/u_s \gg 1$ at rlatively high fields in the low field range and $w_0^2 I/u_s \ll 1$ in the high field range.*

Then, at very low fields, the wall velocity v is expressed by Eq. (5.41), and u_s and I by Eqs. (7.3) and (6.20), respectively. Thus we have, from these equations,

$$v = 2.8 h^{-1/2} b_x^{3/2} b_y b_z^{1/2} P_s^{1/2} I_0^{1/2} \exp(-\Delta\tilde{f}^{\dagger}/2kT) \times \exp\{-b_x b_y(\tilde{\sigma}_f + \sigma_p')/2kT\} \cdot E^{3/4} \exp(-\delta/2E), \tag{9.1}$$

where δ and I_0 are given by Eqs. (6.19) and (6.21), respectively.

At relatively high fields in the low field range, v is given by Eq. (5.21) and I by Eq. (6.20), and $w_0 = 4\sigma''/3P_s E$ as can be seen from Eq. (2.1). Thus we have

$$v = \frac{4}{3} b_x P_s^{-1} I_0 \sigma'' E^{-1/2} \exp(-\delta/E). \tag{9.2}$$

In the high field range, v is given by Eq. (5.41) and u_s and I are expressed by Eqs. (7.2) and (6.39), respectively. Thus v is written as

$$\begin{aligned} v = {} & 1.4\sqrt{2}\, h^{-1} b_x^2 b_y \exp\{-(\Delta f^{\dagger} + \Delta\tilde{f}^{\dagger})/2kT\} \cdot (\tilde{\sigma}_f + \sigma_p' - 2\tilde{i}^{\dagger} P_s b_z E)^{1/2} \\ & \times \{\sigma_f + \sigma_p' - 2i^{\dagger} P_s b_z (E - E')\}^{1/2} \left[\frac{\tilde{\sigma}_f + \sigma_p'}{2P_s b_z E} \exp\{b_x b_y(\tilde{\sigma}_f + \sigma_p')/kT\} \right. \\ & \left. \times \exp\{-2\tilde{i}^{\dagger} P_s b_x b_y b_z E/kT\} - \tilde{i}^{\dagger}\right]^{-1/2} \left[\frac{\sigma_f + \sigma_p'}{2P_s b_z (E - E')} \exp\{b_x b_y(\sigma_f + \sigma_p')/kT\} \right. \\ & \left. \times \exp\{-2i^{\dagger} P_s b_x b_y b_z (E - E')/kT\} - i^{\dagger}\right]^{-1/2}. \end{aligned} \tag{9.3}$$

Eqs. (9.1) and (9.2) show that the field dependence of v in the low field range does not strictly follow the exponential law of the form $v \propto \exp(-\delta/E)$. In fact we have

$$\partial \ln v/\partial(1/E) = -(\delta/2 + 3E/4) \tag{9.4}$$

from Eq. (9.1) and

$$\partial \ln v/\partial(1/E) = -(\delta - E/2) \tag{9.5}$$

from Eq. (9.2). But in this field range the terms $3E/4$ and $-E/2$ are usually small as compared with $\delta/2$ and δ, thus the exponential law approximately holds. However, the activation field defined as $\partial \ln v/\partial(1/E)$ varies with the field and is expected to be nearly twice as greate at a relatively high field as it is at very low fields.

The wall velocity in the high field range expressed by Eq. (9.3) depends on E approximately following a power law. This is obvious from the fact that both

* That this is the case for BT will be shown in the next chapter. However, all the ferroelectrics do not necessarily conform to this schem, since the thickness of the moving wall depends on the relative magnitudes of I, u_s and w_0 and these may differ for different ferroelectrics.

I and u_s, which are respectively given by Eq. (6.39) and Eq. (7.2), vary with E closely following a power law as has been already pointed out in § 6 and 7.

§ 10. Discussions

We have seen in § 5 that, among infinite number of steady states of the thick moving wall, each corresponding to a value of wall velocity in a range, only one state is stable, which corresponds to a wall velocity very close to the lower limit of the range. It is notable that this fact is compatible with the requirement of the thermodynamics of irreversible processes, according to which the stable steady state of a system is characterized by a minimum of entropy production when a linear phenomenological relation exists between the thermodynamic flux and force and the phenomenological coefficient is constant[34)35)].* If these conditions are not fulfilled, the state of minimum entropy production does not necessarily coincide with the steady state.** However, studies of a number of illustrative cases show that the state of minimum entropy production very closely coincides with the steady state even when the conditions are not satisfied[37)]. If we assume that the stable steady state can be approximated by the state of minimum entropy production also in our case of the wall motion, it is expected that among the infinitely many steady states, the stable state will be the one corresponding to a wall velocity close to the minimum of its allowed values, since under the condition that the step structure of the moving wall is time independent the entropy production is caused only by the change of the electrical energy into the internal energy of the crystal and the rate of this change is proportional to the wall velocity.

Another interpretation of fixing the parameter η in Eq. (5.15) as nearly unity is as follows. It has been established in § 5.1 that there exists a stable steady solution for wall motion in which the functions $r(j)$ and $N(j)$ shift with a definite velocity without changing their shapes. The outline of the moving wall displayed on the electroded surface, however, will change with time. But the change will be slow as compared with the nucleation frequency on the top of a salient of the wall. In fact this is verified by the simulations. Thus the wall velocity approximately equals c times the nucleation frequency on the tops. The nucleation frequency is of the order of $w_0 I$, since each top consists of a step whose width hardly exceeds the critical value w_0 as is required by the condition $w_0^2 I/u_s \gg 1$. Thus the wall velocity should be of the order of $cw_0 I$.

Similar interpretation can be given to the formula (5.41) for the velocity of thin walls. In this case, the shapes of the functions $r(j)$ and $N(j)$ will fluctuate with time. Nevertheless it can be said, as an approximation, that the wall velocity is determined by the nucleation on the tops of the protuberances. This time, the average width w' of a top is much greater than w_0, as can be seen from the condition $w_0^2 I/u_s \ll 1$. If the average time interval between a nucleation

* When these conditions are satisfied, there exists only one steady state and this state is stable with respect to perturbations[34)35)]. If there are a number of irreversible processes and also their cross effects, the fulfilment of the Onsager reciprocal relations is additionally required[34)35)].

** For the whole class of macroscopic dissipative and mechanical systems submitted to time independent boundary conditions there exists a criterion of evolution more general than the principle of minimum entropy production[36)].

on a top and the next nucleation on the new top is τ, then we have $w' \approx u_s \tau$ and $w' I \tau \approx 1$, from which we obtain $w' \approx (u_s/I)^{1/2}$. Thus the wall velocity is $v \approx cw'I \approx c(u_s I)^{1/2}$.

The exponential law for the field dependence of the wall velocity in the low field range is replaced by the power law in the high field range. According to the present theory, this change is due to the fact that the two-dimensional nuclei which play the important role at low fields can not be formed at high fields and instead the one-dimensional nuclei nucleate as discussed in detail in §6.2. On the other hand, it is shown that the explanation by Stadler and Zachmanidis[19] of the power law at high fields (§2) is inadequate; numerical calculation for BT indicates that the critical field E'' given by Eq. (6.22) turns out to be 25 kV/cm if σ'' is assumed to be 0.4 erg/cm^2, as done by Stadler and Zachmanidis[19], while the experiments show that the power law is valid at much higher fields (up to 450 kV/cm).

If the nucleation rate I is very low or the length of the wall is very small, situation is quite different from the usual cases discussed in the present chapter; a single nucleus will quickly cover the whole length of the wall before the next nucleation takes place, thus the assumption made by Drougard[24] is now correct. The criterion of the validity of this assumption will be expressed by

$$l \ll l_c, \tag{10.1}$$

where l is the wall length and l_c is a function of I and u_s. The critical length l_c will be given by

$$l_c \approx 1/N_n \approx (u_s/I)^{1/2}, \tag{10.2}$$

where N_n is the number of nucleations per unit length of the wall and given by Eq. (D.4). The expression (10.2) shows that the critical length l_c decreases with increasing field. For BT, the critical length l_c is of the order of microns at the field of 1 esu. We have, however, no experimental data on so small domains that the inequality (10.1) is satisfied.

Originally, the nucleation model was proposed in order to explain the switching of BT[23]. But there is a fair possibility that the switching of some other ferroelectrics also can be explained in terms of the model. The nucleation on an existing wall can occur if the polarization changes its sign discontinuously at the 180° wall. This is true even when the wall has a finite thickness over which the polarization differs considerably from the bulk value. It is evident from the discussions in the preceding sections that, if the nucleation model is valid for a ferroelectric, its wall velocity (and hence the switching rate) must depend exponentially on the field at sufficiently low fields. Thus one of the criteria of the validity of the model is whether the exponential law is followed at low fields. Among the ferroelectrics fulfilling this criterion are TGS[5-7], colemanite[8], thiourea[9], GASH[10-12], etc. At high fields, the present theory predicts that the switching rate follows a power law. This is confirmed experimentally for the above ferroelectrics[5,6,8-12], but the value of the exponent is different for different ferroelectrics. The diversity in the exponent is explicable since according to the present theory the exponent depends on the relative magnitudes of σ_f, σ', $t^\dagger$ etc, and these will differ for different ferroelectrics (§6.2).

Chapter III. Application of General Theory to Barium Titanate

§ 11. Introduction

In the previous chapter, general formulae have been derived for the velocity of the wall motion during ferroelectric switchings. The wall velocity is given by one of Eqs. (9.1) ~ (9.3) according to the field strength.

In the present chapter, we shall apply the general theory to BT and see how various experimental results on this ferroelectric are accounted for by the theory.

§ 12. Comparison with Experimental Data

The wall velocity in BT at room temperature was measured in the low field range by Miller and Savage[16] and in the high field range by Stadler and Zachmanidis[19]. The results are reproduced in Figs. III.1 and III.2 from the original papers.

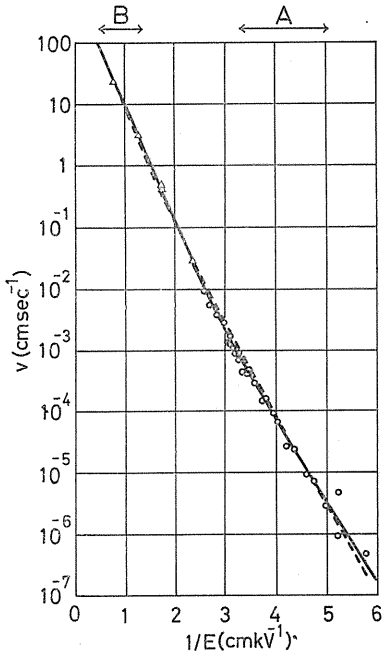

FIG. III.1. Wall velocity v versus reciprocal field $1/E$ in the low field range as reproduced from Miller and Savage's paper[16]. The dotted line represents the theoretical curve. The field ranges A and B are indicated at the top of the figure.

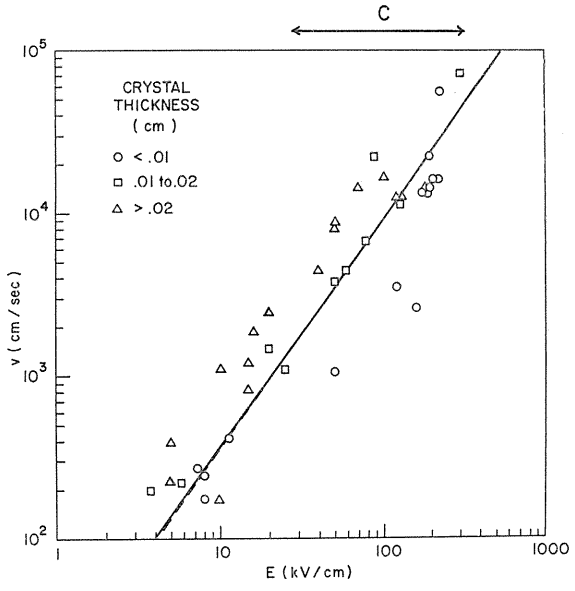

FIG. III.2. Wall velocity v versus field E in the high field range as reproduced from Stadler and Zachmanidis' paper[19]. The dotted line represents the theoretical curve. The field range C is indicated at the top of the figure.

Equations (9.1) ~ (9.3) could be compared immediately with these results if all the constants appearing in the equations were known. However, we have no experimental method of determining directly the boundary energies, the energy barriers, etc. as yet. Furthermore, the present status of microscopic model theories of BT is such that these quantities can only be estimated in the order

of magnitude. We shall therefore determine the values of these quantities by fitting the equations to the experimental curves and see if the obtained values are reasonable.

Let us assume that the wall velocities in the field ranges 200~300 V/cm (range A), 800~2000 V/cm (range B), 30~300 kV/cm (range C) are described by Eqs. (9.1), (9.2) and (9.3), respectively. It should be noted that below 1 kV/cm the experimental data refer to the walls at 45° to the a-axes (110-walls) whereas above 1 kV/cm the data are related with the walls parallel to an a-axis (100-walls) (See §14). We shall further assume that $\sigma_{f100}=\tilde{\sigma}_{f100}=\tilde{\sigma}_{f110}$ $(=\sigma_{f110})$, $i^{\dagger}_{100}=\tilde{i}^{\dagger}_{100}$ and $\Delta f^{\dagger}\approx\Delta\tilde{f}^{\dagger}\ll kT$. Here and in the following the quantities relating to 100-wall are suffixed by 100 and those relating to 110-wall by 110. The depolarizing energy density σ_p is obtained as a function of E from Eqs. (2.1), (2.2) and (6.18), the result being shown in Fig. III.3.

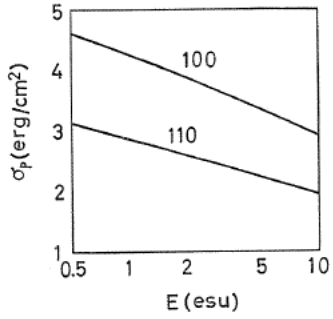

FIG. III.3. Depolarizing energy density σ_p versus field E. The indices represent the orientation of the wall.

Then, the quantities $\sigma_f+\sigma'_p$, σ'_{100}, $i^{\dagger}_{100}$, σ''_{100}, σ''_{110}, $(U_f+\Delta f^*)_{100}$ and $(U_f+\Delta f^*)_{110}$ can be determined by the method of least squares. According to a microscopic theory developed by Kinase *et al.*[38)-40)43)44)], the energy density σ_{100} equals about 1/100 of σ_f. The theory also predicts that $\sigma'_{100}\approx\frac{1}{2}\sigma_{100}$ (Appendix E). Thus σ'_{100} is expected to be about 1/200 of σ_f. If we perform the calculation with the additional condition that $\sigma_f+\sigma'_p=200\,\sigma'_{100}$, we obtain the result*; $\sigma_f+\sigma'_p=41.1$, $\sigma'_{100}=0.205$, $i^{\dagger}_{100}=6.4$, $\sigma''_{100}=0.564$, $\sigma''_{110}=0.916$, $(U_f+\Delta f^*)_{100}=2.64\times10^{-13}$ and $(U_f+\Delta f^*)_{110}=2.06\times10^{-13}$ in cgs units. It is found, from Eq. (6.25), that σ'_p is negligible as compared with σ_f. The microscopic theory of Kinase and others[38)] shows that Δf^* is much smaller than kT for the room temperature, whereas the $(U_f+\Delta f^*)$'s obtained above are substantially greater than kT. Thus we shall neglect σ'_p and Δf^* against σ_f and U_f, respectively. It is seen that $U_{f100}=4.01b^2\sigma_f$ and $U_{f110}=3.13b^2\sigma_f$. The values of σ_f and σ'_{100} are smaller than but of the same order of magnitude as the values calculated from the model theories[38)-41)]. The value of $i^{\dagger}_{100}$ is quite reasonadle[38)40)].

The wall velocity caluculated from Eqs. (9.1)~(9.3) using the values obtained above are shown by the dotted lines in Figs. III.1 and III.2. The calcu-

* The experimental curve of Fig. III.1 in the field range 1~2 kV/cm (for 100-wall) is not accurate because of insufficient data in that range, hence the obtained values of σ''_{100} and U_{f100} may involve considerable errors. These errors, however, do not affect the accuracy of the values of the other quantities.

lated values of $w_0^2 I/u_s$ are shown in Fig. III. 4, which verifies the assumption that Eqs. (9.1)~(9.3) are valid respectively in the field ranges A, B and C.

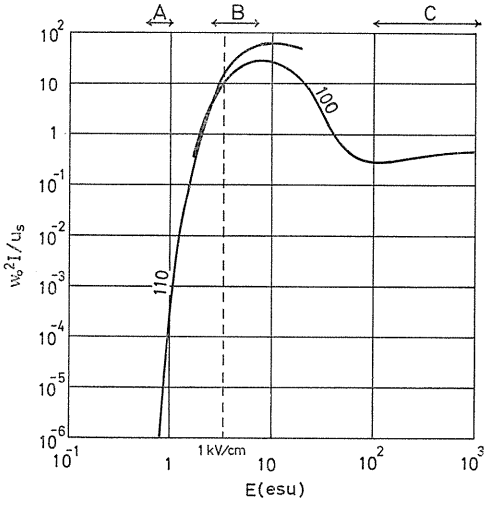

FIG. III. 4. Calculated value of $w_0^2 I/u_s$ versus field E. The indices represent the orientation of the wall. The field ranges A, B and C are indicated at the top of the figure.

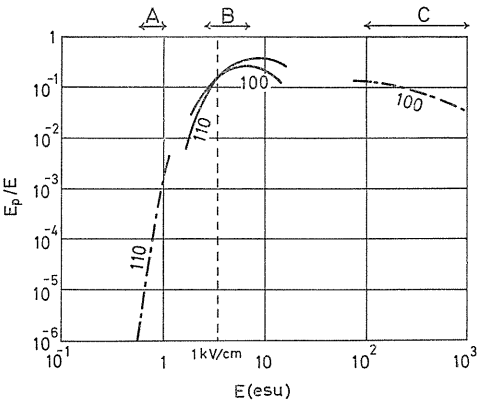

FIG. III. 5. Calculated value of opposite field E_p versus applied field E. The broken lines represent the upper limit to E_p. The indices represent the orientation of the wall. The field ranges A, B and C are indicated at the top of the figure.

§ 13. Effect of Polarization Charges

The effect of the polarization charges has been discussed in § 8, according to which the upper limit to the opposite field E_p created at the electrode by the polarization charges is given by Eq. (8.6) in the field ranges A and C while the field E_p is given by Eq. (8.9) in the field range B.

The result of numerical calculation is shown in Fig. III. 5. The parameter γ and the inclination of the side boundary $\tan\theta$ were assumed to be 2 and 1/10, respectively, in the calculation. It is seen that E_p is negligible in the field ranges A and C. In the field range B, it is not negligible, which indicates that the result of the preceding section should be modified if the effect of the polarization charges is taken into account. However, the effect of E_p shown in Fig. III. 5 is not serious even in the field range B. Furthermore, in Eq. (8.9) the value of E_p is overestimated; in reality the polarization charges must be largely compensated by the free charges in the crystal. Thus, in the following, we shall neglect the effect of the polarization charges.

§ 14. Field Dependence of Relative Velocities of 100- and 110-Walls

It is known that the domains in BT grow at room temperature in the form of square, the orientation of which is field dependent; the 110-wall appear at lower fields and the 100-walls appear at higher fields, and at the intermediate field of about 1 kV/cm, the walls of both orientations are observed, the shape of the domains becoming octagonal[16)42)]. This fact indicates that

$$\left.\begin{aligned} &v_{100} > v_{110} \quad \text{when} \quad E < 1 \text{ kV/cm}, \\ &v_{100} < v_{110} \quad \text{when} \quad E > 1 \text{ kV/cm} \end{aligned}\right\} \quad \text{and} \quad \left\{\begin{aligned} &\\ &v_{100} = v_{110} \quad \text{when} \quad E \approx 1 \text{ kV/cm}, \end{aligned}\right\} \tag{14.1}$$

where v represents the wall velocity. The difference in wall velocity due to the orientation becomes less conspicuous at high temperatures[42].

The critical field 1 kV/cm is in the field range B where v is described by Eq. (9.2). If Eq. (9.2) is written in the form

$$v = v_0 E^{1/2} \exp(-\delta/E),$$

the constants v_0 and δ vary with the orientation dependent quantities c, σ'' and U_f as

$$v_0 = \text{const}\, c^{9/4} \sigma''^{3/4} \exp(-U_f/kT),$$
$$\delta = \text{const}\, c^{3/2} \sigma''^{3/2},$$

where c is the minimum advancement of wall. Thus it is necessary that

$$2^{1/2} \sigma''_{100} < \sigma''_{110}, \tag{14.2}$$

$$\sigma''_{100} \exp(-4U_{f100}/3kT) < 2^{-3/2} \sigma''_{110} \exp(-4U_{f110}/3kT) \tag{14.3}$$

in order that $v_{100} > v_{110}$ at lower field and $v_{100} < v_{110}$ at higher fields, since $c_{100} = b$ and $c_{110} = b/\sqrt{2}$ (Fig. III. 6). The values of the quantities determined in § 12 conform to the requirements (14.2) and (14.3) and the insertion of those values into Eqs. (9.1) and (9.2) yields the result which satisfies the condition (14.1) in the field ranges A and B.

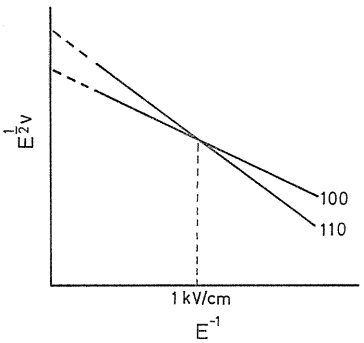

FIG. III. 6. Wall velocities v_{100} and v_{110} multiplied by the square root of the field E as functions of the reciprocal field $1/E$ in the field range B.

For the inequality $v_{100} < v_{110}$ to be satisfied in the high field range, however, the result of § 12 should be modified. Numerical examination of Eq. (9.3) reveals that there is an upper limit to σ_{f110} for the condition $v_{100} < v_{110}$ to be satisfied. Here the v_{100} is assumed to be given by the experimental curve in Fig. III. 2. The upper limit is dependent on σ'_{110} and increases with decreasing σ'_{110} approaching 26.7 erg/cm^2 at the limit of $\sigma'_{110} \to 0$. Thus, retaining the values relating to 100-wall and assuming that $\sigma'_{110} = \sigma'_{100}/\sqrt{2}$ as is shown in Appendix E on the basis

of the theory by Kinase *et al.*[39)43)44)].* we shall modify the values for 110-wall and choose the following set of values; $\sigma_{f100}=41.1$, $\sigma'_{100}=0.205$, $i^{+}_{100}=6.4$, $\sigma''_{100}=0.564$, $U_{f100}=2.64\times10^{-13}$, $\sigma_{f110}=25.0$, $\sigma'_{110}=0.146$, $i^{+}_{110}=4.1$, $\sigma''_{110}=0.934$ and $U_{f110}=2.00\times10^{-13}$ in cgs units. These modifications result in a less satisfactory fit to the data in the low field range, although the discrepancy is still small. A value near the upper limit is chosen for σ_{f110}, since the larger σ_{f110} is the better is the fit in the low field range. The values chosen above are found to satisfy the condition (14.1) throughout the field ranges *A*, *B* and *C*.

The observed diminution with increasing temperature of the difference in wall velocity due to the orientation is explicable since the quantities σ_f, σ'' and U_f influence the wall velocity mainly through the factors of the form exp (const $\times\sigma_f/kT$), etc..

§ 15. Side Boundary Energy Dependent on Slanting Angle

In Eqs. (9.1) and (9.2), on which the discussions in the preceding sections are based, the energy σ'' is assumed constant. In reality, the energy σ'' must be dependent on the slanting angle θ. This dependency may be particularly strong for a ferroelectric like BT in which the anisotropy is large. However, microscopic treatment of a slanting boundary is a very complicated problem.

Thus, in this section, we shall take into account the θ-dependence of σ'' tentatively assuming that σ'' is given by

$$\sigma''=\sigma'(1+p\theta^2) \tag{15.1}$$

for small θ, where p is positive, and see how the results of the preceding sections are modified.

Then the free energy increment associated with the formation of a triangular nucleus of width $2a$ and height l equals

$$\Delta F=-2P_sEalc+2c\sigma'\left(1+p\frac{a^2}{l^2}\right)(a^2+l^2)^{1/2}+2\sigma_p ca^2/l, \tag{15.2}$$

from which we obtain the dimensions and the free energy of the critical nucleus:

$$a^*=2\sigma'/3P_sE, \tag{15.3}$$

$$l^*=2\sigma'^{1/2}(p\sigma'+\sigma_p)^{1/2}/\sqrt{3}P_sE, \tag{15.4}$$

$$\Delta F^*=8c\sigma'^{3/2}(p\sigma'+\sigma_p)^{1/2}/3\sqrt{3}P_sE. \tag{15.5}$$

Here, anticipating that $p\gg1$, the unity in the second term on the right hand side of Eq. (15.2) has been neglected against pa^2/l^2.

Thus, Eqs. (6.14), (6.15), (6.16), (6.19) and (6.21) are replaced respectively by

$$A=8b_x(b_yb_z)^{1/2}p^{1/4}\sigma'/3^{3/4}kT, \tag{15.6}$$

$$s=2\times3^{1/4}p^{1/4}, \tag{15.7}$$

---

* According to the microscopic theory by Lawless[41)], σ'_{110} is supposed to be greater than σ'_{100}. If σ'_{110} is taken to be greater than assumed here, the smaller becomes the upper limit to σ_{f100}.

$$i^* = 4p^{1/2}\sigma'^2/3\sqrt{3}\,b_y b_z P_s^2 E^2, \tag{15.8}$$

$$\delta = 8b_x\sigma'^{3/2}(p\sigma' + \sigma_p)^{1/2}/3\sqrt{3}\,P_s kT, \tag{15.9}$$

$$I_0 = \left(\frac{2\sqrt{3}}{\pi}\right)^{1/2}\frac{(kT)^{1/2}}{h}(b_x b_y b_z)^{1/2}P_s^{1/2}p^{1/4}n_1\exp\left(-\frac{4f^*}{kT}\right)\exp\left(-\frac{U_f}{kT}\right). \tag{15.10}$$

Comparison of Eqs. (15.9) and (15.10) with Eqs. (6.19) and (6.21) shows that we can obtain as good a fit to the data as in § 14, retaining the values of σ_f, σ' and $i^\dagger$ determined there and putting $p_{100}=4.32\times10^2$, $p_{110}=5.02\times10^3$, $U_{f100}=3.06\times10^{-13}$ erg and $U_{f110}=2.77\times10^{-13}$ erg.

§ 16. Conclusions and Discussions

We have seen that the general formulae (9.1) ~ (9.3) successfully explain both the absolute value and the field dependence of the observed wall velocity in BT over a wide range of field by the use of reasonable values of the constants. The field dependence of the domain orientation is also accounted for by the formulae. For this it is necessary that $\sigma''_{100}<\sigma''_{110}$ and $\sigma_{f100}>\sigma_{f110}$. A possible physical interpretation of the latter inequality is that the step height ($=c$) is smaller and hence σ_f is more easily reduced by the rotation of P_s at the boundary for the 110-walls. The microscopic treatment of the bouudary energies σ'' and σ_f is a rather complicated problem and has not been worked out as yet.

There are a number of experimental facts which can not be accounted for by the nucleation model alone; the so called Miller effect[17], the dependence on the crystal thickness of the wall velocity[18)45)] and the transient phenomena at the beginning of the wall motion[46)47)]. These effects seem to have an additional source, which most probably is the conductivity in the crystal. The Miller effect can be qualitatively explained in terms of the free charges drawn by the polarization charges and trapped at the imperfections behind the moving wall, while the other two effects are explained in terms of the surface charge layers the formation of which has been established experimentally[48)49)]. Detailed discussions of these problems, however, will not be given here.

Chapter IV. Temperature and Pressure Dependence of Activation Field

§ 17. Introduction

According to the general theory of sidewise wall motion during switching, which has been developed in Chap. II, the wall velocity depends exponentially on the field in the low field range at fixed temperature and pressure and the activation field δ is determined by the boundary energy σ'', the dielectric constant ε, the temperature T, etc., depending on these quantities following the formula

$$\delta = \text{const}\,\sigma''^{3/2}/(\varepsilon_a\varepsilon_b)^{1/4}T. \tag{17.1}$$

where ε_a and ε_b are the dielectric constants in the directions of the two principal axes of the dielectric ellipsoid ot the crystal which are perpendicular to the ferroelectric axis. Therefore, one of the ways to examine the model will be to compare the temperature or pressure dependences of δ and $\sigma''^{3/2}/(\varepsilon_a\varepsilon_b)^{1/4}T$,

However, we have no experimental method of determining the boundary energy σ''. There are several theoretical studies of the boundary energy, all of which indicate that σ'' is proportional to the square of the spontaneous polarization P_s. Thus Eq. (17.1) can be rewritten in the form

$$\delta = \text{const}\, P_s^3/(\varepsilon_a\varepsilon_b)^{1/4}T. \qquad (17.2)^*$$

It is experimentally easier to measure the activation field for the switching rate α than to measure the activation field for the wall velocity δ (§1). It is shown, from the consideration of domain kinetics, that α and δ have a close relation with each other and proportionality exists between the two activation fields[15)19)21)]. Thus the comparison can also be made between α and $P_s^3/(\varepsilon_a\varepsilon_b)^{1/4}T$.

Savage and Miller[50)] measured the wall velocity in BT over a temperature range covering most of the tetragonal region and compared the temperature dependences of δ and $P_s^3/\varepsilon_a^{1/2}T$.** The result showed a rough agreement between the experiment and the theory. However, little can be said about the measure of the agreement because the variation in this temperature range of the right hand side of Eq. (17.2) is mainly through the factor $P_s^3/\varepsilon_a^{1/2}$ rather than the accurately determinable factor T^{-1}, there being considerable disagreement in the reported data of P_s and ε_a especially in the vicinity of the Curie point[50)51)]. In this respect TGS will be more suitable for the study since it suffers no phase transition below the Curie point and both P_s and ε vary very slowly with T in the wide low temperature region[52)53)] over which T^{-1} is varied by a considerable factor.

In the next section is presented a measurement of the switching rate of TGS over a temperature range from 87 K to the room temperature and the temperature dependence of α is compared with the theory. A measurement of P_s in the same temperature range is also described.

Wieder[8)] carried out a measurement on colemanite and obtained both P_s and α as functions of T. Using these data we examine in similar way the agreement between experiment and theory for this ferroelectric (§19).

As for the pressure dependence we have no available quantitative data. In §20, some experiments on the effect of hydrostatic pressure will be described and the results compared with the theory. The experiment has been done on BT as well as on TGS.

§18. Temperature Dependence of the Activation Field for TGS

18.1. Experimental

The *b*-plates approximately 0.3 mm in thickness were cut from a mother crystal grown from aqueous solution by the cooling method below the Curie point. Evaporated gold films were used as the electrodes. The temperature of the sample was controlled by a cryostat, liquid nitrogen being used as the cryogen. Alternate positive and negative square pulses were used to switch the

* In §15 we took into account the dependence of σ'' on the slanting angle θ in a particular way and obtained Eq. (15.9), according to which δ is approximately proportional to σ''^2 since the second term will usually be small as compared with the first in the parentheses on the right hand side of the equation. Hence in Eq. (17.2) the exponent 3 of P_s should be replaced by 4. However, this change does not seriously affect the conclusion of this chapter.

** Here ε_a is the dielectric constant in the direction of the *a*-axes.

samples. The signal was generated by means of a mercury relay. The ratio of the pulse width to the rest time was unity except for very long pulses for which the rest time was limited to 2 min. The switching pulse was observed on an oscilloscope when the switching time was relatively short, while a recorder was used for very slow switchings. The switching time t_s and the peak current i_m were measured as functions of the field and the temperature. Then the activation field α was obtained as a function of the temperature from the data of t_s and i_m.

The spontaneous polarization P_s was measured on low frequency hysteresis loops. The frequency of the switching signal was always 0.022 sec^{-1}. The output of the Sawyer-Tower circuit was connected with the input of an X-Y recorder through an electrometer. In order to avoid the error due to the switching outside the electroded portion, the sample was electroded on the whole area of the b-faces.

18.2. Result

The temperature depemdence of P_s are shown in Fig. IV.1. It is found that the present values coincide at very low temperatures with the values of P_s calculated by Chynoweth from his pyroelectric data[52]. Near the Curie point, however, the present values exceed Chynoweth's and also those obtained by Hoshino *et al.*[53].

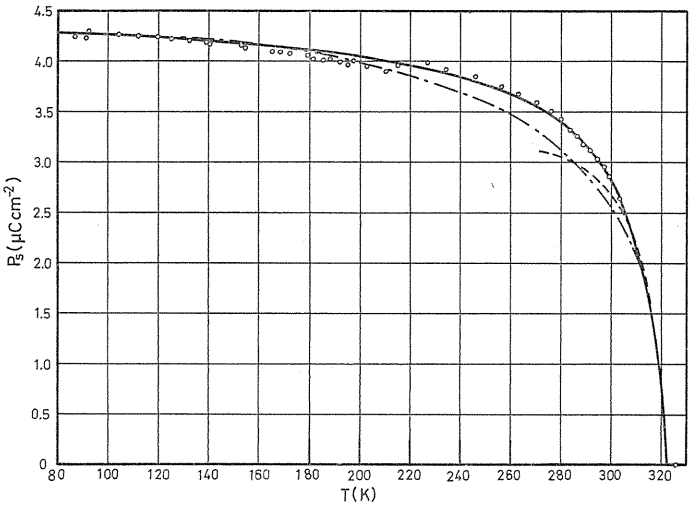

FIG. IV.1. Plot of the spontaneous polarization P_s versus temperature T for TGS.

The data of α for two samples are shown in Fig. IV.2. Among the quantities appearing on the right hand side of Eq. (17.2), which is to be compared with data, the dielecreic constants are practically constant over the whole temperature range of the measurements[53]. Therefore the temperature dependence of α should be compared with that of P_s^3/T. The quantity P_s^3/T is calculated using the P_s data of Fig. IV.1 and plotted versus T in Fig. IV.2 on a scale which is suitable for the comparison. The solid curve shows this result. The magnitude

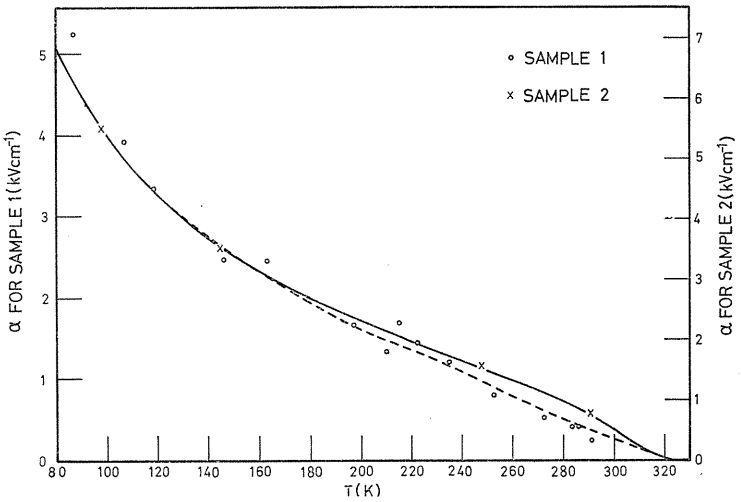

FIG. IV.2. Plot of the activation field α versus temperature T for TGS and the curves showing $P_s^3T^{-1}$ versus T which are drawn in arbitrary units. The circles and the crosses indicate the experimental points for α. The solid curve is for $P_s^3T^{-1}$ calculated from the curve of Fig. IV.1, while the dashed curve is for $P_s^3T^{-1}$ calculated from Chynoweth's data[52].

of P_s^3/T calculated from Chynoweth's values of P_s is also shown as the dashed curve in the same figure for the comparison. The scale factor is different for the two curves. A fairly good agreement is found between the curves representing P_s^3/T and the experimental points for α.

§ 19. Argument Based on Wieder's Data on Colemanite

Wieder's plots of $P_s(T)$ and $\alpha(T)$ for colemanite are respectively reproduced on Figs. IV.3 and IV.4. For this ferroelectric, no data are available for the dielectric constants in the directions perpendicular to the ferroelectric axis. It is supposed, however, that the variation with temperature of the dielecreic constants is not large, since usually the dielectric constants do not vary appreciably below the Curie temperature except in the vicinity of the Curie point. In addition, the small absolute value of the exponent makes the factor $(\varepsilon_a\varepsilon_b)^{-1/4}$ less

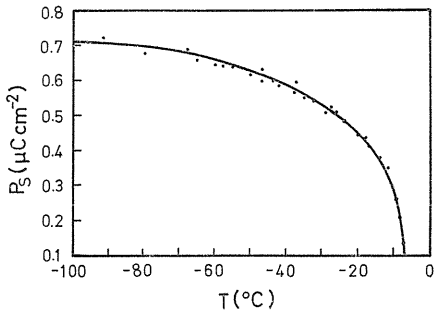

FIG. IV.3. Plot of the spontaneous polarization P_s versus temperature T for colemanite. This is the reproduction from Wieder's paper[8].

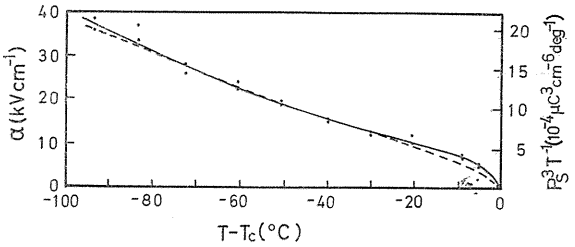

FIG. IV.4. Plot of the activation field α versus temperature T for colemanite (the points and the solid curve), which is the reproduction from Wieder's paper[8], and the curve showing $P_s^3T^{-1}$ versus T (the dashed curve) calculated from the curve of Fig. IV.3.

important as compared with the other factors in the right hand side of Eq. (17.2). Thus we shall compare the temperature dependences of α and P_s^3/T. The latter is calculated using the values of P_s shown in Fig. IV.3 and is represented by the dashed curve in Fig. IV.4. The comparison of the curves in Fig. IV.4 shows that the agreement is good also for this ferroelectric.

§ 20. Effect of Hydrostatic Pressure on the Switching Rates of BT and TGS

20.1. Experimental

Pure single crystals of BT were grown by the Remeika method[54]. Most crystals had a thickness in the neighbourhood of 0.1 mm. Single crystals of TGS were grown by the same method as described in § 18.1, and *b*-plates approximately 0.2 mm thick were cut from the crystals. Evaporated gold film was used as the electrode for both BT and TGS. For BT, however, evaporated silver film, NaCl solution and liquid mercury were also used as the electrode for comparison. Hydrostatic pressure up to 2 kbar was produced by a hand pump which was connected with the sample chamber by a steel capillary. The sample chamber was a steel vessel of single cylinder type Silicone oil was used as the pressure transmitter. The electrical leads passed through the plug by means of the pipestone-cone method[55]. The switching time t_s and the peak current i_m were measured at the room temperature as functions of the field and the pressure by the same method as described in § 18.1, then the activation field α were obtained as functions of the pressure.

20.2. Result

It has been found that the activation field α decreases with the pressure p for BT and increases with p for TGS (Figs. IV.5 and IV.6). The pressure dependences are linear within the studied pressure range. There is no systematic difference due to different material of the electrode. The observed fractional rates of change are

$$(\partial\alpha/\partial p)/\alpha = -(5.0 \pm 0.9) \times 10^{-11}, \tag{20.1}$$

$$(\partial\alpha/\partial p)/\alpha = (8.5 \pm 1.3) \times 10^{-11}, \tag{20.2}$$

for BT and TGS, respectively, in cgs unit. On account of these changes in α, the switching rate is increased and decreased for BT and TGS, respectively, by the application of the pressure.

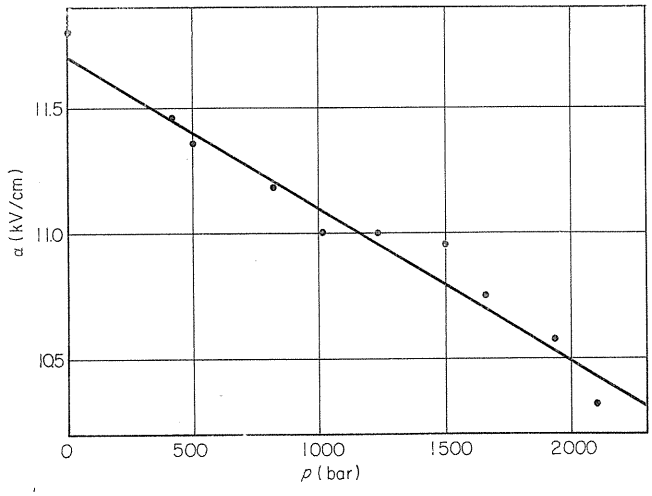

FIG. IV.5. Typical plot of activation field α versus hydrostatic pressure p for BT.

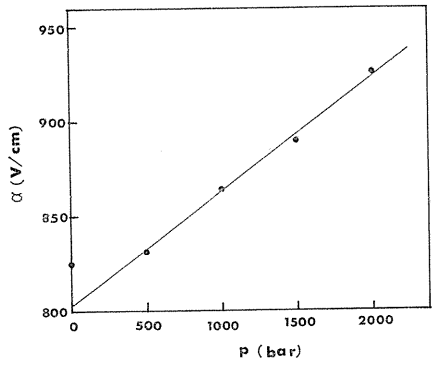

FIG. IV.6. Typical plot of activation field α versus hydrostatic pressure p for TGS.

Among the quantities appearing on the right hand side of Eq. (17.2), the change with pressure of $(\varepsilon_a\varepsilon_b)^{1/4}$ is estimated to be small in comparison with that of P_s^3 for both ferroelectrics. Thus the experimental results (20.1) and (20.2) are to be compared with the fractional rates of change with p of the spontaneous polarizations multiplied by 3. Dependences on hydrostatic pressure of P_s have been measured for BT by Samara[56] and for TGS by Jona and Shirane[57]. The results are

$$(\partial P_s/\partial p)/P_s = -1.7\times10^{-11}, \tag{20.3}$$

$$(\partial P_s/\partial p)/P_s = 2.6\times10^{-11}, \tag{20.4}$$

for BT and TGS, respectively, in cgs unit. Equations (20.1)~(20.4) show that there is an excellent agreement between the experiment and the theory for both ferroelectrics (Table IV.1).

TABLE IV. 1. Comparison between the Fractional Rates of Change with Hydrostatic Pressure p of the Activation Field α and the Spontaneous Polarization P_s for BT and TGS

	$\{(\partial\alpha/\partial p)/\alpha\}_{p=0}$ (cgs)	$3\{(\partial P_s/\partial p)/P_s\}_{p=0}$ (cgs)
BT	$-(5.0\pm0.9)\times10^{-11}$	-5.1×10^{-11}
TGS	$(8.5\pm1.3)\times10^{-11}$	7.8×10^{-11}

§ 21. Discussion and Conclusion

Equation (17.2), an important prediction of the nucleation model for the wall motion in ferroelectric switching, has been verified by the experiments described in this section, in which the quantities on both sides of the equation have been varied through temperature and pressure variation and compared with each other. The results thus provide an evidence in favour of the model. In particular, the temperature dependence of α for TGS and colemanite indicates that the wall motion is a process due to thermal agitation, since in these cases the change of the right hand side of the equation is mainly through the factor T^{-1} which originates in the assumption of thermal activation process.

Chapter V. Conclusion

Detailed theoretical study has been made of the nucleation model for wall motion in ferroelectrics. Kinetics of the wall motion has been worked out both analytically and by simulation. The wall velocity is expressed in terms of the nucleation rate and the sideways growth velocity of nuclei on the wall. The latter two quantities have been calculated on the basis of the theory of absolute reaction rates. From these results, general formulae for absolute wall velocity in various field ranges have been derived. These formulae indicate that the field dependence of the wall velocity follows the exponential law in the low field range and the power law in the high field range, in agreement with the experimental result.

According to the present theory, the different field dependences in different field ranges are due to the fact that two-dimensional nuclei nucleate at low fields while one-dimensional nuclei are formed at high fields. In the low field range, where the exponential law is valid, the activation field increases with increasing field. This is accounted for by the present theory in terms of the change in the relative effectiveness of the nucleation and the sideways growth of the nuclei on the wall. The present theory also tells us that the exponent characterizing the power law holding in the high field range depends on the front boundary energy, the side boundary energy, the critical size, etc. of the one-dimensional nuclei. This accounts for the experimental fact that the exponent differs for different ferroelectrics.

Numerical discussion for barium titanate shows that the general formulae for wall velocity successfully explain both the absolute value and the field dependence of the observed wall velocity in this ferroelectric over a wide range

of field. The field dependence of the domain orientation is also accounted for by the formulae.

The temperature dependence of the activation field of triglycine sulphate was studied over a temperature range from 87 K to the room temperature, and the result was compared with the prediction of the nucleation model. Similar comparison was made for colemanite using Wieder's data. The pressure dependence of the activation field was also studied for barium titanate and triglycine sulphate under a hydrostatic pressure up to 2 kbar at the room temperature and comparison was made between the experiment and the theory. All these results show that the agreement is good.

Acknowledgments

The author wishes to express his sincere thanks to Professor Ryuji Abe for the valuable discussions. He is also indebted to Professor I. Ninomiya for the discussions about the differential equations. The simulations described in Chapter II were performed by the use of FACOM 230-60 of Hokkaido University and other numerical calculations as well as the analyses of the expermental data were made using FACOM 230-60's of Kyoto University and of Nagoya University and HITAC 5020 E of Tokyo University. The author is grateful to Mr. S. Hirano for his help in constructing the pressure apparatuses and the cryostat used in the experiments described in Chapter IV. The content of Chapter II has been published in Journal of the Physical Society of Japan, Vol. 33, No. 3, p. 616, 1972. The content of Chapter IV has been published in Journal of the Physical Socety of Japan, Vol. 26, No. 5, p. 1163, 1969; Vol. 31, No. 5, p. 1450, 1971 and Vol. 33, No. 3, p. 739, 1972.

Appendix A. Solution of Simultaneous Differential Equations (5.11) and (5.12)

Equations (5.11) and (5.12) are rewritten as

$$\begin{cases} f' = Pg & \text{(A.1)} \\ g' = Qg + R\dfrac{g^2}{1-f} & \text{(A.2)} \end{cases}$$

with

$$P = -2u_s/(v - cw_0 I), \quad \text{(A.3)}$$

$$Q = -2cIu_s/v(v - cw_0 I), \quad \text{(A.4)}$$

$$R = 2u_s/v. \quad \text{(A.5)}$$

The differentiation of Eq. (A.1) yields

$$f'' = Pg'. \quad \text{(A.6)}$$

Inserting Eqs. (A.1) and (A.6) into Eq. (A.2), we have

$$\frac{f''}{f'} - Q = -\frac{R}{P}\frac{f'}{f-1}, \quad \text{(A.7)}$$

which can be integrated, yielding

$$\ln|f'| - Qx = -\frac{R}{P}\ln|f-1| + C, \tag{A.8}$$

where C is the constant of integration.

Since our solution for the steady state must satisfy the conditions $0 \leq f \leq 1$ and $f' \leq 0$, Eq. (A.8) should be written as

$$\ln(-f') - Qx = -\frac{R}{P}\ln(1-f) + C, \tag{A.9}$$

Which can be transformed into

$$-(1-f)^{R/P}f' = C'/\exp(Qx), \tag{A.10}$$

where $C' = \exp(C)$ is a positive constant.

Equation (A.10) can be integrated and we obtain

$$\frac{1}{R/P+1}(1-f)^{R/P+1} = \frac{C'}{Q}\exp(Qx) + C'', \tag{A.11}$$

where C'' is another constant of integration. From Eqs. (A.3) and (A.5) it is found that

$$R/P + 1 = cw_0I/v > 0 \tag{A.12}$$

for positive v. Thus Eq. (A.11) can be solved for f, and the result is

$$f = 1 - \left[\left(\frac{R}{P}+1\right)\left\{\frac{C'}{Q}\exp(Qx) + C''\right\}\right]^{\frac{1}{R/P+1}}. \tag{A.13}$$

If it is assumed that $v < cw_0I$, Eq. (A.4) requires that $Q > 0$, from which it must follow that the second term in the right hand side of Eq. (A.13) becomes infinitely great in the limit of $x \to \infty$, as can be seen from the inequality (A.12) and the fact that C' is positive. Therefore if must be that

$$v > cw_0I \tag{A.14}$$

in order that the solution possesses the required properties. When inequality (A.14) is satisfied, we have, from Eqs. (A.3) ~ (A.5),

$$1/(R/P+1) > 1, \qquad Q < 0. \tag{A.15}$$

The constants C' and C'' are determined by the boundary conditions $f(0) = 1$ and $f(\infty) = 0$. The results are

$$C' = -Q/(R/P+1), \tag{A.16}$$

$$C'' = 1/(R/P+1). \tag{A.17}$$

Inserting Eqs. (A.16) and (A.17) into Eq. (A.13), we obtain

$$f = 1 - \{1 - \exp(Qx)\}^{\frac{1}{R/P+1}}. \tag{A.18}$$

The function $g(x)$ is obtained by differentiating $f(x)$, as can be seen from Eq. (A.1), thus we obtain, using Eq. (A.18),

$$g=\frac{1}{P}f'$$

$$=\frac{Q}{R+P}\exp(Qx)\{1-\exp(Qx)\}^{-\frac{R}{R+P}}, \tag{A.19}$$

in which we find

$$\frac{Q}{R+P}>0, \qquad -\frac{R}{R+P}>0, \tag{A.20}$$

from Eqs. (A.3)~(A.5) and inequality (A.14).

Inspection of Eqs. (A.18) and (A.19) reveals, by the help of Eqs. (A.15) and (A.20), that the solution given by Eqs. (A.18) and (A.19) satisfies all of the boundary conditions (5.14) provided that the inequality (A.14) is satisfied.

Thus we find that there exists a solution to the simultaneous equations (5.11) and (5.12), which satisfies the boundary conditions (5.14), for an arbitrary value of v provided that $v>cw_0I$. For a value of v which is equal to

$$v=\eta cw_0I, \tag{A.21}$$

where $\eta>1$, the solution is given by

$$f=1-\{1-\exp(-x/\lambda)\}^{\eta}, \tag{A.22}$$

$$g=\frac{1}{w_0}\exp(-x/\lambda)\{1-\exp(-x/\lambda)\}^{\eta-1}, \tag{A.23}$$

where

$$\lambda=\eta(\eta-1)\frac{w_0^2I}{u_s}c, \tag{A.24}$$

as can be seen by inserting Eq. (A.21) into Eqs. (A.18) and (A.19) and using Eqs. (A.3)~(A.5).

Appendix B. Calculation of Depolarizing Energy due to the Polarization Charge on the Boundaries of a Nucleus

B.1. Calculation by Miller and Weinreich

Miller and Weinreich[23] calculated, for BT, the depolarizing energy of a triangular nucleus, approximating the polarization charges on the two slanting side boundaries by two linear charges and integrating the energy of interaction between the charge elements;

$$U_d=\int\frac{q_1q_2}{\varepsilon r_{12}}dx_1dx_2, \tag{B.1}$$

and obtained, neglecting the effects of the image forces from the electrode,

$$= U_d \frac{8P_s^2a^2b^2}{\varepsilon_a l}\left\{\ln\left(\frac{2a}{b}\right)-1\right\},$$

where $2a$ and l are respectively the width and the height of the triangle, but this result contains a calculative error. The correct result is

$$U_d = \frac{8P_s^2a^2b^2}{\varepsilon_a l}\left\{\ln\left(\frac{\varepsilon_a l^2}{\varepsilon_c ab}\right)-1\right\}.$$

Actually, however, the self energy of a linear charge is infinitely great. In the above calculations, the lower limit for r_{12} in Eq. (B.1) has been arbitrarily taken to be b in order to avoid the divergence. A more reasonable way will be to approximate the polarization charges by cylindrical charge distributions of appropriate radius In the following, calculation will be made employing this approximation.

B.2. Energies of linear charges

B.2.1. Self energy of a linear charge

Suppose that the charge be distriburd uniformly in a cylinder of length l and radius a (Fig. B.1) placed in a homogeneous and isotropic medium of di-elecreic constannt ε and the linear density of the charge measured along the axis of the cylinder be q. If a is much smaller than l, the electrostatic energy outside the cylinder* can be calculated to be

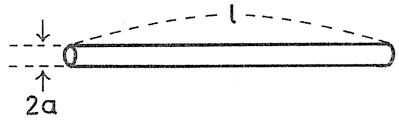

FIG. B.1. Long cylindrical charge distribution of length l and radius a.

$$U = \frac{q^2}{\varepsilon} l \ln(l/a), \tag{B.2}$$

approximating the cylinder by a long ellipsoid.

B.2.2. Interaction energies of pairs of linear charges

The interaction energies of pairs of linear charges disposed variously against each other can be calculated by integrating the interaction energies between the charge elements on both lines [cf. Eq. (B.1)]. The linear densities of the two

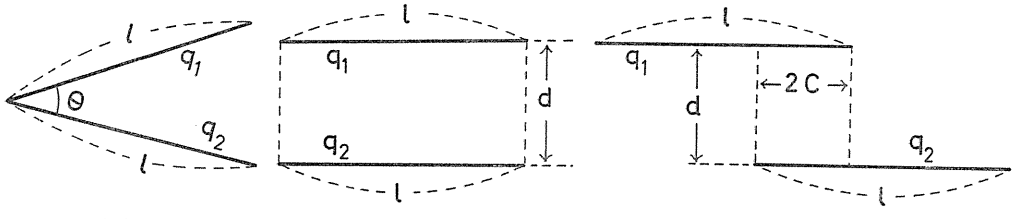

(a) (b) (c)

FIG. B.2. (a) Two linear charges having a common end. (b) Two parallel linear charges, case I. (c) Two parallel linear charges, case II.

* The energy inside the cylinder should be included in the boundary energy and not in the depolarizing energy.

linear charges are assumed to be q_1 and q_2, respectively.

(a) Two linear charges having a common end (Fig. B.2a)

$$U_{12}=2\frac{q_1q_2}{\varepsilon}l\ln\left(1+\operatorname{cosec}\frac{\theta}{2}\right). \tag{B.3}$$

(b) Two parallel linear charges, case I (Fig. B.2b)

$$U_{12}=2\frac{q_1q_2}{\varepsilon}\left\{l\ln\frac{l+\sqrt{l^2+d^2}}{d}-\sqrt{l^2+d^2}+d\right\}. \tag{B.4}$$

(c) Two parallel linear charges, case II (Fig. B.2c)

$$\begin{aligned}U_{12}=2\frac{q_1q_2}{\varepsilon}\Bigg[&l\ln\frac{2(l-c)+\sqrt{\{2(l-c)\}^2+d^2}}{l-2c+\sqrt{(l-2c)^2+d^2}}\\&+c\ln\left(\frac{2c+\sqrt{(2c)^2+d^2}}{2(l-c)+\sqrt{\{2(l-c)\}^2+d^2}}\frac{\{l-2c+\sqrt{(l-2c)^2+d^2}\}^2}{d^2}\right)\\&-\frac{1}{2}\sqrt{\{2(l-c)\}^2+d^2}-\frac{1}{2}\sqrt{(2c)^2+d^2}+\sqrt{(l-2c)^2+d^2}\Bigg].\end{aligned} \tag{B.5}$$

B.3. Depolarizing energies of nuclei

B.3.1. Treatment of electrostatic problem in anisotropic medium

In an anisotropic medium like a crystal the dielectric constant is not a scalar but a tensor. If the principal axes ot the tensor are respectively called a, b and c-axis, the relation between the field E and the electric displacement D is expressed by

$$D_a=\varepsilon_aE_a,\qquad D_b=\varepsilon_bE_b,\qquad D_c=\varepsilon_cE_c, \tag{B.6}$$

and the basic equation for the electrostatic field is

$$\varepsilon_a\frac{\partial^2\phi}{\partial a^2}+\varepsilon_b\frac{\partial^2\phi}{\partial b^2}+\varepsilon_c\frac{\partial^2\phi}{\partial c^2}=4\pi\rho, \tag{B.7}$$

where ϕ is the electrostatic potential and ρ the charge density.

If we make a transformation $a,\ b,\ c\rightarrow a',\ b',\ c'$ such that

$$a'=a,\qquad b'=m_2b,\qquad c'=m_3c, \tag{B.8}$$

where

$$m_2=(\varepsilon_a/\varepsilon_b)^{1/2},\qquad m_3=(\varepsilon_a/\varepsilon_c)^{1/2}, \tag{B.9}$$

then we have, from Eq, (B.7),

$$\varepsilon_a\Delta'\phi=4\pi\rho, \tag{B.10}$$

in which Δ' stands for $\partial^2/\partial a'^2+\partial^2/\partial b'^2+\partial^2/\partial c'^2$.

Eqnation (B.10) indicates that the problem is reduced to an isotropic problem in a homogeneous medium of dielectric constant ε_a, with the same values of ϕ and ρ. It can be shown by simple calculations that, if Q, U and u represent total charge and energy in a finite volume and energy density, respectively, and the

corresponding quautities in the transformed system are denoted by primed characters,* we have the relations

$$\phi' = \phi, \tag{B.11}$$

$$E'_a = E_a, \quad E'_b = E_b/m_2, \quad E'_c = E_c/m_3, \tag{B.12}$$

$$\rho' = \rho, \tag{B.13}$$

$$Q' = m_2 m_3 Q, \tag{B.14}$$

$$u' = u, \tag{B.15}$$

$$U' = m_2 m_3 U. \tag{B.16}$$

Thus we know that, when the problem is treated in the transformed system, the values of the charge density and the energy density are unaltered while the total charge and the total energy are multiplied by $m_2 m_3$.

B.3.2. Triangular nucleus

The depolarizing energy is caused by the polarization charges on the two side boundaries Q_1 and Q_2 and their images Q_3 and Q_4 (Fig. B.3). If we denote the self energy of Q_i by $U(Q_i)$ and the interaction energy of Q_i and Q_j by $U(Q_i, Q_j)$, the depolarizing energy is written as

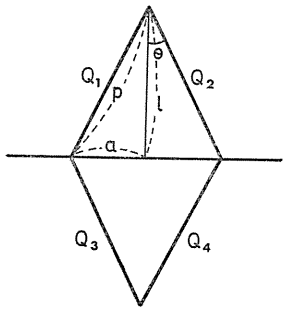

FIG. B.3. Polarization charges Q_1 and Q_2 on a triangular nucleus and their images Q_3 and Q_4.

$$U_d = \frac{1}{2}\left\{\sum_i U(Q_i) + \sum_{i>j} U(Q_i, Q_j)\right\}. \tag{B.17}$$

We can calculate the depolarizing energy in the transformed isotropic system U'_d, each term on the right hand side of Eq. (B.17) being calculated by the use of Eqs. (B.2) ~ (B.5). Then U_d is obtained by dividing U'_d by $m_2 m_3$ in accordance with Eq. (B.16). The result is

$$U_d = 2\sigma_p b_x a^2/l, \tag{B.18}$$

in which

$$\sigma_p = \frac{4P_s^2 b_x}{(\varepsilon_a \varepsilon_b)^{1/2}}\left[\ln\left\{\left(\frac{2}{\mu}\right)^{1/2} \frac{(\varepsilon_a \varepsilon_b)^{3/4}}{\varepsilon_c(\varepsilon_a \cos^2\varphi + \varepsilon_b \sin^2\varphi)^{1/2}} \frac{l^2}{a(b_x b_y)^{1/2}}\right\} - 2\ln 2\right], \tag{B.19}$$

* The definitions for the quantities in the transformed system are:

$$E'_a = -\frac{\partial \phi'}{\partial a'}, \text{ etc.}; \quad Q' = \int \rho' da' db' dc'; \quad U' = \frac{1}{8\pi}\int E' \cdot D' da' db' dc.$$

where μ represents the thickness of the slanting side boundaries measured in b_y (Fig. B.4) and φ is the angle between the a- and the x-axis in the xy- (or ab-) plane (Fig. B.5). The ferroelectric axis is assumed to be parallel to the c- (or z-) direction. In calculating Eqs. (B.18) and (B.19), a^2 has been neglected against l^2.

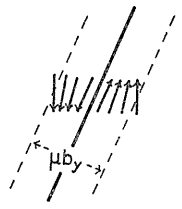

FIG. B.4. Thickness of a slanting side boundary, over which the polarizations are rotated.

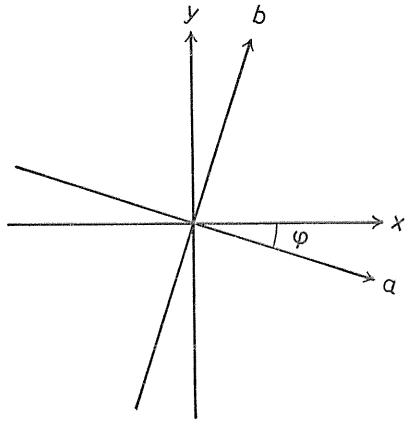

FIG. B.5. Angle φ between the direction of wall motion x and one of the dielectric principal axes a. The spontaneous polarizatios is parallel to the z- (or c-) axis.

In Eq. (B.19), the second term in the square bracket is due to the interaction betweem the polarization charges and their images. Numerical examination for BT reveals that for $\varphi=0$ the second term amounts to 13.5% of the first at $E=1$ esu and 16.0% at $E=5$ esu.

B.3.3. Rectangular nucleus

The depolarizing energy is caused by the polarization charge Q_1 on the front boundary and its image Q_2 (Fig. B.6). In similar way to the preceding sub-

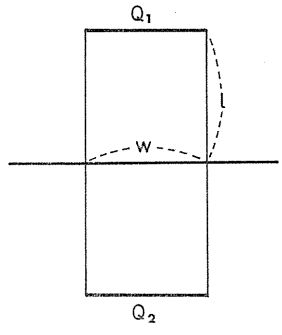

EIG. B.6. Polarization charge Q_1 on a rectangular nucleus and its image Q_2.

section, we obtain

$$U_d = \sigma_p b_x w, \tag{B.20}$$

were

$$\sigma_p = \frac{4P_s^2 b_x}{\varepsilon_c^{1/2}(\varepsilon_a\cos^2\varphi+\varepsilon_b\sin^2\varphi)^{1/2}}\left[\ln\left\{\left(\frac{2}{\nu}\right)^{1/2}\frac{\varepsilon_c^{1/4}(\varepsilon_a\cos^2\varphi+\varepsilon_b\sin^2\varphi)^{3/4}}{(\varepsilon_a\varepsilon_b)^{1/2}}\frac{w}{(b_xb_y)^{1/2}}\right\}\right.$$
$$\left.-\frac{\varepsilon_c^{1/2}(\varepsilon_a\cos^2\varphi+\varepsilon_b\sin^2\varphi)^{1/2}}{4(\varepsilon_a\varepsilon_b)^{1/2}}\frac{w}{l}\right]. \tag{B.21}$$

Here ν is half the thickness of the front boundary measured in b_z. In the calculation, w^2 has been neglected against l^2.

B.3.4. One-dimensional nucleus

The depolarizing energy is caused by the polarization charge at the point like front boundary, the volune of which we shall approximate by an ellipsoid of minor radius $(b_xb_y)^{1/2}/2$ and major radius νb_z (Fig. B.7). The result of the calculation is

FIG. B.7. Approximation of the charge distribution at the front boundary of a one-dimensional nucleus by an ellipsoid.

$$U_d = b_xb_y\sigma_p', \tag{B.22}$$

where

$$\sigma_p' = \frac{P_s^2 b_x b_y}{2\pi\nu(\varepsilon_a\varepsilon_b)^{1/2}b_z}\ln\frac{4\nu(\varepsilon_a\varepsilon_b)^{1/4}b_z}{\varepsilon_c^{1/2}(b_xb_y)^{1/2}}. \tag{B.23}$$

Appendix C. Calculation of A, B, s, i^* and ΔF^* in Eqs. (6.14) ~ (6.17)

The increase in free energy associated with the formation of a triangular nucleus of width $2a$, height l and thickness b_x is written as[23]

$$\Delta F = -2P_sEalb_x + 2\sigma''b_x(a^2+l^2)^{1/2} + U_f + U_d, \tag{C.1}$$

where U_f represents the extra energy existing at the top of the nucleus* and the depolarizing energy U_d is given by Eq. (B.18). The first term on the right

* Miller and Weinreich neglected this term.

hand side of Eq. (C.1) is the bulk energy and the second and the third term represent the boundary energy. The dimensions a^* and l^* and the free energy ΔF^* of the critical nucleus are determined by the conditions $\partial\Delta F/\partial a=0$ and $\partial\Delta F/\partial l=0$, which yield (§ 2)

$$a^* = 2\sigma''/3P_sE, \tag{C.2}$$

$$l^* = 2\sigma''^{1/2}\sigma_p^{1/2}/3^{1/2}P_sE, \tag{C.3}$$

$$\Delta F^* = 8b_x\sigma''^{3/2}\sigma_p^{1/2}/3^{3/2}P_sE + U_f. \tag{C.4}$$

In the calculation a^2/l^2 and σ''/σ_p have been neglected against unity.

The number of unit cells existing in a triangular nucleus of dimensions l, $2a$ and b_x is equal to

$$i = al/b_yb_z. \tag{C.5}$$

If it is assumed that the triangle is always similar to that for the critical nucleus, we have

$$l/a = l^*/a^* = (3\sigma_p/\sigma'')^{1/2}, \tag{C.6}$$

by the use of Eqs. (C.2) and (C.3).

Equation (C.1) can be rewritten, by the use of Eqs. (B.18), (C.5) and (C.6), in the form

$$\Delta F = U_f + (8/3^{3/4})b_x(b_yb_z)^{1/2}\sigma''^{3/4}\sigma_p^{1/4}i^{1/2} - 2EP_sb_xb_yb_zi. \tag{C.7}$$

Comparing Eq. (C.7) with Eq. (6.2), we have

$$A = (8/3^{3/4})b_x(b_yb_z)^{1/2}\sigma''^{3/4}\sigma_p^{1/4}/kT, \tag{C.8}$$

$$B = 2EP_sb_xb_yb_z/kT. \tag{C.9}$$

The number of unit cells existing along the boundaries of a nucleus is approximately equal to $2(a^2+l^2)^{1/2}/(b_yb_z)^{1/2}$, which can be rewritten as $2(3\sigma_p/\sigma'')^{1/4}i^{1/2}$ by the use of Eqs. (C.5) and (C.6). Thus we have

$$s_1 \approx s_2 \approx s \approx 2(3\sigma_p/\sigma'')^{1/4}. \tag{C.10}$$

The volume of the critical nucleus is equal to

$$V^* = a^*l^*b_x. \tag{C.11}$$

Therefore we have

$$i^* = V^*/b_xb_yb_z = a^*l^*/b_yb_z = (4/3^{3/2})\sigma''^{3/2}\sigma_p^{1/2}/b_yb_zP_s^2E^2, \tag{C.12}$$

by the use of Eqs. (C.2) and (C.3).

Appendix D. Number of Steps per Unit Length of Thin Moving Wall

The number of nuclei formed during a time interval dt is

$$dN' = I(1-\theta)dt, \tag{D.1}$$

where the reversed fraction θ is given by

$$\begin{aligned}\theta &= 1-(1-\theta_0)\exp(-2N_0u_st-w_0It-u_sIt^2)\\ &\approx 1-(1-\theta_0)\exp(-u_sIt^2),\end{aligned} \tag{D.2}$$

from Eqs. (5.31) and (5.32). The total number of nucleations during t_1 is calculated to be

$$\begin{aligned}N' &= \int dN' = \int_0^{t_1} I(1-\theta)\,dt\\ &= (1-\theta_0)I\int_0^{t_1}\exp(-u_sIt^2)\,dt\\ &= (1-\theta_0)(I/u_s)^{1/2}\int_0^{\rho-\theta_0}\exp(-x^2)\,dx\\ &\approx (1-\theta_0)(I/u_s)^{1/2},\end{aligned} \tag{D.3}$$

by the use of Eqs. (5.39), (D.1) and (D.2). Hence the number of nucleations per unit length of the wall is

$$N_n = N'/(1-\theta_0) \approx (I/u_s)^{1/2}. \tag{D.4}$$

The number of side boundaries per unit length of the wall is of the order of but smaller than $2N_n$, thus

$$N_B \lesssim 2(I/u_s)^{1/2}. \tag{D.5}$$

Appenbix E. Relation between σ and σ' for BT

The side boundary of a two- or one-dimensional nucleus is very different from a usual 180° wall. We shall discuss this problem for an infinite crystal on the basis of the theory due to Kinase *et al.*[39)43)44)] and show that σ' is considerably smaller than σ.

According to the theory, the coefficient of dipole interaction for a Ti ion is given by

$$a' = -\gamma(ne)^2/2\alpha_{Ti},$$

where ne is the effective charge of a Ti ion, α_{Ti} its polarizability and γ represents the specific dipole interaction for the polarization state under consideration.* The principle of superposition tells us that the dipole interaction γ experienced by a Ti ion is written as

$$\gamma = \sum_j \Gamma_j, \tag{E.1}$$

where Γ_j denotes the dipole interaction exerted on the Ti ion by the shift of the ions in j-th column of the crystal. Anticipating that Γ's due to distant colums are small, we shall calculate Γ's only for the first and the second neigh-

* The polarization state is determined when the sign of the polarization is fixed in every unit cell in the crystal.

bour columns, neglecting the Γ's from the higher order neighbour columns. It will be advantageous to utillze the result of Kinase's calculation[43] of the dipole interactions in the ferroelectric and two kinds of antiferroelectric states of the crystal (Fig. E. 1), according to which the dipole interactions in these states are respectively $\gamma_{\text{ferro}}=0.1974$, $\gamma_{\text{stripe}}=0.1969$, $\gamma_{\text{checker}}=0.1969$. These γ's can be expressed in terms of Γ's as

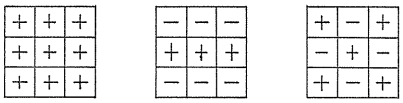

FIG. E. 1. Polarization configuration in the ferroelectric and two kinds of antiferroelectric states.

$$\gamma_{\text{ferro}}=\Gamma_0+4\Gamma_1+4\Gamma_2, \tag{E.2a}$$

$$\gamma_{\text{stripe}}=\Gamma_0-4\Gamma_2, \tag{E.2b}$$

$$\gamma_{\text{checker}}=\Gamma_0-4\Gamma_1+4\Gamma_2. \tag{E.2c}$$

Here Γ_0, Γ_1 and Γ_2 are the dipole interactions from the column in which the Ti ion exists and a first and a second neighbour column, respectively (Fig. E. 2). Solving Eqs. (E. 2a) ~ (E. 2c) for Γ_0, Γ_1 and Γ_2, we obtain

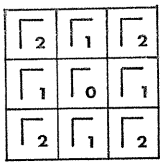

FIG. E. 2. Symbols representing the dipole interactions experienced by a Ti ion in the central column due to the polarization of the same column and the first and the second neighbour rcolumns.

$$\Gamma_0=(\gamma_{\text{ferro}}+2\gamma_{\text{stripe}}+\gamma_{\text{checker}})/4=0.1970, \tag{E.3a}$$

$$\Gamma_1=(\gamma_{\text{ferro}}-\gamma_{\text{checker}})/8=0.000062, \tag{E.3b}$$

$$\Gamma_2=(\gamma_{\text{ferro}}+\gamma_{\text{checker}}-2\gamma_{\text{stripe}})/16=0.000031. \tag{E.3c}$$

The dipole interaction experienced by a Ti ion in a 100-wall is written as

$$\gamma_0=\Gamma_0+2\Gamma_1. \tag{E.4}$$

The dipole interaction energy per unit cell in bulk is equal to

$$U_{\text{bulk}}=-\gamma_{\text{ferro}}\frac{(ne)^2}{2\alpha_{\text{Ti}}}x^2, \tag{E.5}$$

while the energy per unit cell in a 100-wall is

$$U_{\text{wall}}=-\gamma_0\frac{(ne)^2}{2\alpha_{\text{Ti}}}x^2, \tag{E.6}$$

where x is the shift of the Ti ions and assumed to be constant in the approximation of the present treatment. Since a 100-wall is two lattice constants thick in our approximation (Fig. E.3), the wall energy equals

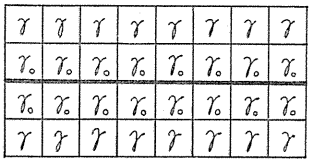

FIG. E.3. Dipole interaction experienced by a Ti ion in each column in the neighbourhood of a 100-wall. γ stands for γ_{ferro}.

$$\sigma_{100} = 2(U_{\text{wall}} - U_{\text{bulk}})/b^2 = S(4\Gamma_1 + 8\Gamma_2), \tag{E.7}$$

where S is given by

$$S = (ne)^2 x^2 / 2b^2 \alpha_{\text{Ti}}. \tag{E.8}$$

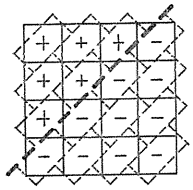

(a)

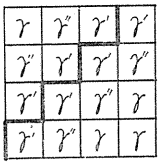

(b)

FIG. E.4. Polarization configuration (a) and dipole interaction in each column (b) in the neighbourhood of a 110-wall. γ stands for γ_{ferro}.

A 110-wall is shown in Figs. E.4a and E.4b. In Fig. E.4b, the dipole interaction experienced by Ti ions in each column is shown. The symbols γ' and γ'' represent

$$\gamma' = \Gamma_0 + 2\Gamma_2, \tag{E.9}$$

$$\gamma'' = \Gamma_0 + 4\Gamma_1 + 2\Gamma_2, \tag{E.10}$$

respectively. From the figure we see that the increase in dipole interaction energy caused by the presence of the wall equals, per length $\sqrt{2}b$ of the wall,

$$b^2 S\{4\gamma_{\text{ferro}} - (2\gamma' + 2\gamma'')\}, \tag{E.11}$$

which can be calculated to be

$$b^2 S(8\Gamma_1 + 8\Gamma_2), \tag{E.12}$$

by the use of Eqs. (E.2a), (E.9) and (E.10). Thus we have, for the wall energy of a 110-wall,

$$\sigma_{110} = S(8\Gamma_1 + 8\Gamma_2)/\sqrt{2}. \tag{E.13}$$

The numerical calculation of Eqs. (E.7) and (E.13) yields $\sigma_{100} = 1.4$ and $\sigma_{110} = 1.5$, both in erg/cm^2.

Now we shall calculate the side boundary energies of two- and one-dimensional nuclei formed on 180° wall. It will be assumed that the nuclei are of infinite height and their side boundaries are parallel to the polar axis. First we shall consider a one-dimensional nucleus on a 100-wall. As can be seen from Fig. E.5, the dipole interaction on Ti ions changes in 9 columns surrounding the nucleus as the result of the formation of the nucleus, in our first and second neighbour approximation. In Fig. E.5. the dipole interaction in each column is indicated for the states before and after the formation of the nucleus. The symbol γ'' is given by Eq. (E.10) and γ''' by

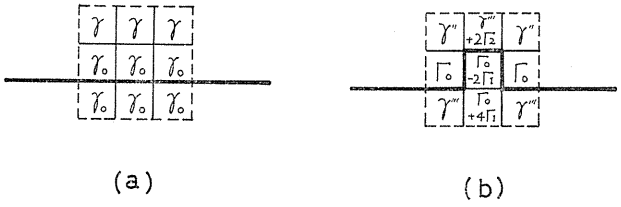

FIG. E.5. Dipole interaction in each column before (a) and after (b) the formation of a one-dimensional nucleus on a 100-wall. γ stands for γ_{ferro}.

$$\gamma''' = \Gamma_0 + 2\Gamma_1 + 2\Gamma_2. \tag{E.14}$$

Thus the increase in dipole interaction energy associated with the formation of a one-dimensional nucleus is

$$b^2S[(3\gamma_{\text{ferro}} + 6\gamma') - \{2\Gamma_0 + (\Gamma_0 - 2\Gamma_1) + (\Gamma_0 + 4\Gamma_1) + (\gamma''' + 2\Gamma_2) + 2\gamma'' + 2\gamma'''\}] = 8b^2S\Gamma_1 \tag{E.15}$$

per length b of the nucleus. Since the energy given by Eq. (E.15) is shared between the two side boundaries of the nucleus, the effective boundary energy of the nucleus equals

$$\sigma'_{100} = 4S\Gamma_1. \tag{E.16}$$

Similarly, we can calculate the effective boundary energy of a two-dimensional nucleus formed on a 100-wall. Then we find that the boundary energy is always given by Eq. (E.16) irrespective of the width of the nucleus. In Fig. E.6, di-

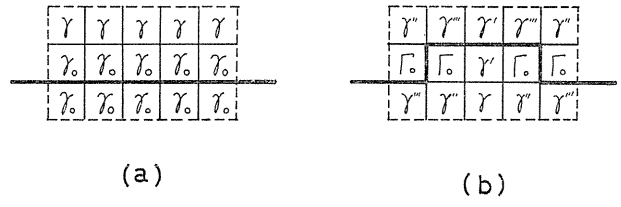

FIG. E.6. Dipole interaction in each column before (a) and after (b) the formation of a two-dimensional nucleus of width $3b$ on a 100-wall. γ stands for γ_{ferro}.

pole interaction in each column is indicated for the states before and after the formation of a two-dimensional nucleus of width $3b$.

The formation of a two-dimensional nucleus on a 110-wall can be treated in similar way. Figures E.7 and E.8 show the formation of a one-dimensional nucleus and a two-dimensional nucleus of width $3\sqrt{2}b$, respectively. We see that the thickness of the nuclei is equal to $b/\sqrt{2}$. We can calculate the increment of dipole interaction energy associated with the formation of the nuclei in the same way as in the case of the nuclei on 100-walls, and find that the effective boundary energy of a two- or one-dimensional nucleus on a 110-wall always equals

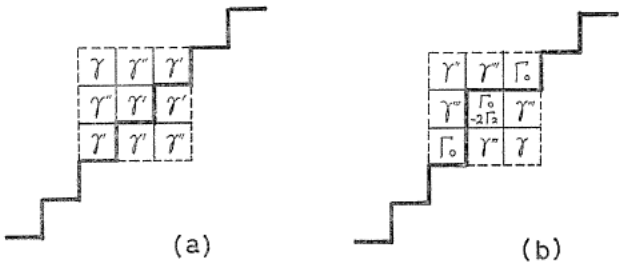

FIG. E.7. Dipole interaction in each column before (a) and after (b) the formation of a one-dimensional nucleus on a 110-wall. γ stands for γ_{ferro}.

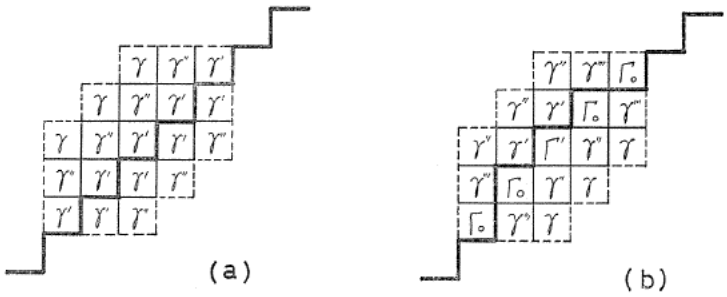

FIG. E.8. Dipole interaction in each column before (a) and after (b) the formation of a two-dimensional nucleus of width $3\sqrt{2}b$ on a 110-wall. γ stands for γ_{ferro}.

$$\sigma'_{110} = 4\sqrt{2}\,S\Gamma_2. \tag{E.17}$$

If we assme that $\gamma_{\text{stripe}} = \gamma_{\text{checker}}$ in accordance with Kinase's result mentioned earlier, although the number of figures is not sufficient, then we have $\Gamma_1 = 2\Gamma_2$, which yields, together with Eqs. (E.7), (E.13), (E.16) and (E.17),

$$\sigma'_{100}/\sigma_{100} = 1/2, \tag{E.18}$$

$$\sigma'_{110}/\sigma_{110} = 1/3, \tag{E.19}$$

$$\sigma'_{110}/\sigma'_{100} = 1/\sqrt{2}. \tag{E.20}$$

References

1) W. J. Merz: Phys. Rev., **95** (1954), 690.
2) E. A. Little: Phys. Rev., **98** (1955), 978.
3) H. H. Wieder: J. Appl. Phys., **27** (1956), 413.
4) H. L. Stadler: J. Appl. Phys., **29** (1958), 1485.
5) C. F. Pulvari and W. Kuebler: J. Appl. Phys., **29** (1958), 1742.
6) E. Fatuzzo and W. J. Merz: Phys. Rev., **116** (1959), 61.
7) H. H. Wieder: J. Appl. Phys., **35** (1964), 1224.
8) H. H. Wieder: J. Appl. Phys., **31** (1960), 180.
9) G. J. Goldsmith and J. G. White: J. Chem. Phys., **31** (1959), 1175.
10) H. H. Wieder: Proc. Inst. Radio Engrs., **45** (1957), 1094.
11) M. Prutton: Proc. Phys. Soc. (London), **B 70** (1957), 1064.
12) E. Fatuzzo: Helv. Phys. Acta, **33** (1960), 429.
13) discussed in, for instance, E. Fatuzzo and W. J. Merz: *Ferro-electricity* (North-Holland Pub. Co. Amsterdam, 1967), Chap. 7, § 3.1.
14) R. C. Miller: Phys. Rev., **111** (1958), 736.
15) R. C. Miller and A. Savage: Phys. Rev., **112** (1958), 755.
16) R. C. Miller and A. Savage: Phys. Rev., **115** (1959), 1176.
17) R. C. Miller and A. Savage: Phys. Rev. Letters, **2** (1959), 294.
18) R. C. Miller and A. Savage: J. Appl. Phys., **31** (1960), 662.
19) H. L. Stadler and P. J. Zachmanidis: J. Appl. Phys., **34** (1963), 3255.
20) M. Hayashi and H. Mishima: Japan J. Appl. Phys., 8 (1969), 968.
21) E. Fatuzzo: Phys. Rev., **127** (1962), 1999.
22) R. Landauer: J. Appl. Phys., **28** (1957), 227.
23) R. C. Miller and G. Weinreich: Phys. Rev., **117** (1960), 1460.
24) M. E. Drougard: J. Appl. Phys., **31** (1960), 352.
25) R. E. Nettleton: J. Appl. Phys., **38** (1967), 2775.
26) H. L. Stadler: J. Appl. Phys., **37** (1966), 1947.
27) R. Abe: J. Phys. Soc. Japan, **14** (1959), 633.
28) H. L. Stadler: Buturi, **21** (1966), 404 [in Japanese].
29) M. Avrami: J. Chem. Phys., **7** (1939), 1103.
30) M. Avrami: J. Chem. Phys., **8** (1940), 212.
31) M. Avrami: J. Chem. Phys., **9** (1941), 177.
32) D. Turnbull and J. C. Fisher: J. Chem. Phys., **17** (1949), 71.
33) S. Glasstone, K. J. Laidler, and H. Eyring: *The Theory of Rate Processes* (McGraw-Hill, New York, 1941).
34) I. Prigogine: *Iutroduction to Thermodynamics of Irreversible Processes* (Interscience Publishers, New York, 1961).
35) S. R. de Groot and P. Mazur: *Non-Equilibrium Thermodyuamics* (North-Holland, Amsterdam, 1962).
36) P. Glansdorff and I. Prigogine: Physica, **30** (1964), 351.
37) C. Kittel: *Elementary Statistical Physics* (John Wiley and Sons, New York, 1967).
38) W. Kinase, A. Kazami, and S. Yokoyama: J. Phys. Soc. Japan, **28**, Supple. (1970), 343.
39) W. Kinase and H. Takahasi: J. Phys. Soc. Japan, **12** (1957), 464.
40) W. Kinase: Busseiron Kenkyu, **4** (1958), No. 5 [in Japanese].
41) W. N. Lawless: Phys. Rev., **175** (1968), 619.
42) H. L. Stadler and P. J. Zachmanidis: J. Appl. Phys., **35** (1964), 2895.
43) W. Kinase: Progr. Theor. Phys., **13** (1955), 529.
44) W. Kinase and H. Takahasi: J. Phys. Soc. Japan, **10** (1955), 942.
45) W. J. Merz: J. Appl. Phys., **27** (1956), 938.
46) R. C. Miller and A. Savage: J. Appl. Phys., **32** (1961), 714.
47) D. R. Callaby: J. Appl. Phys., **36** (1965), 2751.

48) R. Williams: J. Phys. Chem. Solids, **26** (1965), 399.
49) H. Motegi: J. Phys. Soc. Japan, **32** (1972), 202.
50) A. Savage and R. C. Miller: J. Appl. Phys., **31** (1960), 1546.
51) W. J. Merz: Phys. Rev., **91** (1953), 513; T. S. Benedict and J. L. Durand: Phys. Rev., **109** (1958), 1091; V. N. Murzin and A. I. Demeshina: Soviet Physics-Solid State, **6** (1964), 144.
52) A. G. Chynoweth: Phys. Rev., **117** (1960), 1235.
53) S. Hoshino, T. Mitsui, F. Jona, and R. Pepinsky: Phys. Rev., **107** (1957), 1255.
54) J. P. Remeika: J. Am. Chem. Soc., **76** (1954), 940.
55) P. W. Bridgman: *The Physics of High Pressure* (G. Bell and Sons, London, 1958), Chap. 2, p. 30.
56) G. A. Samara: Phys. Rev., **151** (1966), 378.
57) F. Jona and G. Shirane: Phys. Rev., **117** (1960), 139.